Synthesis, Characterization and Applications of Microsphere-Supported Biomembranes

by

Bin He

A Dissertation Submitted to the Graduate Faculty in Engineering in Partial Fulfillment of the requirements for the Degree of Doctor of Philosophy, The City University of New York

2011

This manuscript has been read and accepted for the

Graduate Faculty in Engineering in satisfaction of the

dissertation requirement for the degree of Doctor of Philosophy.

Prof. M. Lane Gilchrist

_____	_____
Date	Chair of Examining Committee

Prof. Mumtaz Kassir

_____	_____
Date	Executive Officer

Prof. Alexander Couzis

_____

Prof. Charles Maldarelli

_____

Prof. David H. Calhoun

_____

Prof. Sihong Wang

_____

Supervisory Committee

THE CITY UNIVERSITY OF NEW YORK

Abstract

Synthesis, Characterization and Applications of Microsphere-Supported Biomembranes

by

Bin He

Advisor: Prof. M. Lane Gilchrist

Our objective is to develop a microsphere-based platform for assaying the function, interactions, and inhibition of membrane proteins. To functionalize such materials with active membrane proteins, the challenge is to build stabilized, microsphere-supported biomembranes in which the substrate to biomembrane spacing can be controlled to accommodate larger membrane proteins. These systems are termed proteolipobeads or lipobeads depending on the constituents.

The silica microsphere (4.7 micron) surface was functionalized with DiNHS-PEG in order to make a tethering bridge designed to yield greater spacing. Confocal fluorescence microscopy was utilized to analyze the silica surface at different stages of surface modification and examine the passivation of the substrate and the formation of lipid bilayers. The lateral mobility and fluidity of the supported membranes was analyzed using fluorescence recovery after photobleaching (FRAP). Flow cytonmetry and Fluorescence Activated Cell Sorting (FACS) was used as a biomembrane quality control measure, an important advantage of the lipobead

format.

These structures have been employed as a route to functionally immobilize the yeast drug efflux pump PDR5, an important anti-fungal drug target. Another intention is to develop a new platform to present molecules to stem cells within a biomimetic architecture: as laterally-mobile molecules embedded in the context of a tailored biomembrane.

Preface

This thesis describes an experimental study on the synthesis, characterization and application of supported biomembrane microsphere assemblies, termed proteolipobeads (PLBs) Our objective is to develop a highly miniaturized, solid-phase platform for assaying the function, interactions and inhibition of integral membrane proteins. To functionalize materials with active membrane proteins, the challenge is to build stabilized, supported biomembranes in which the substrate to biomembrane spacing can be controlled to accommodate larger membrane proteins. The present study is focused on the implementation of a biomimetic approach to create microsphere-supported membranes. These structures have been employed as a route to functionally immobilize the yeast drug efflux pump PDR5, an important anti-fungal drug target. Another intention is to develop a new platform to present molecules to stem cells within a biomimetic architecture: as laterally-mobile molecules embedded in the context of a tailored biomembrane. We have used DiNHS-PEG based conjugates to anchor the lipid bilayer supporting the silica microspheres. This work can be divided into three major parts, synthesis and characterization of supported biomenbrane microsphere assemblies, fabrication of lipid bilayers on containing the yeast drug efflux pump PDR5, and the creation of biomimetic cell-to-cell interactions within human mesenchymal stem cell niches.

In chapter 1, we described the basic motivation of our work. Background information on the lipids and the lipid bilayer assemblies has been provided. We have discussed the numerous issues related to the use of membrane proteins for various applications. i.e. membrane protein PDR5 as drug efflux pump and cell adhesion protein N-Cadherin on biomimetic ligand presentation within the stem cell niche. Our strategy to fabricate functional and stable biomembrane microspheres assemblies has been described. The overall objectives of this

project have been discussed. Meanwhile, the basic information on fluorescence and confocal microscopy and flow cytometry has been provided. The Fluorescence Recovery after Photobleaching (FRAP) technique has also been introduced.

Chapter 2 introduced yeast *S. cerevisiae* cell culture and PDR5 GFP fusion protein purification. Affinity separation and multi-scale chromatographic purification methods have been discussed. We also utilized a microfluidic device for monitoring upregulation of PDR5 GFP. At the same time, experimental analytical SDS-PAGE gel electrophoresis and western blotting techniques using antibodies specific to the target protein have been explained.

In chapter 3, we have discussed the details of synthesis and characterization of tether supported beads. The modification of silica microsphers surface using Di-NHS-PEG and Biotin-PEG-NHS has been introduced. Different strepavidin-coated quantum dots were used as markers to detect the biotin-PEG anchor. Laterally fluidity of the fluorescently tagged lipids was analyzed using FRAP technique and was compared with the case of untethered lipid bilayer on plain silica bead surface. FACS has been used as an important tool for proteolipobeads characterization.

Chapter 4 deals with human mesenchymal stem cell culture and biomimicry of cell-to-cell interactions in a collagen matrix. A brief literature review of stem cell 2D culture and how to build stem cell niches in 3D has been discussed. Detailed hMSC culture has been introduced. The fabrication of the N-Cadherin proteolipobeads has been included in this chapter. MESF kits were applied for N-Cadherin coverage analysis. The creation of hMSC-proteolipodbead-collagen hybrid matrices has been described. Live and dead stem cell staining was applied in collagen matrices to evaluate cell viability. CLSM 3D reconstruction was obtained to analyze the MSC-PLB interactions.

Chapter 5 gives the overall objective of this project and an overview of the results

achieved in the current thesis. Future works such as encapsulation of collagen gel are described in the final part of the thesis.

Acknowledgments

First and foremost I offer my sincerest gratitude to my supervisor, Professor M. Lane Gilchrist, who has supported me throughout my thesis with his patience and knowledge whilst allowing me the room to work in my own way. I attribute the level of my Ph.D degree to his encouragement and effort and without him this thesis, too, would not have been completed. One simply could not wish for a better supervisor.

I thank Professor Sihong Wang for offering techniques and materials for the stem cell project. I thank Professor David H. Calhoun for the equipment of high-speed centrifuge helping out the PDR5 project. I thank Professor Charles Maldarelli for his recommendation on my dissertation fellowship. I thank Professor Alexander Couzis for providing a safe and comfortable working place during my pregnancy. I would like to show my gratitude to all professors in our department.

The Department of Chemical Engineering has provided the support and equipment I have needed to produce and complete my thesis. Thanks to Xu, Andy and Lisa.

In my daily work I have been blessed with a friendly and cheerful group of fellow students. Thanks to my lab mate Lina Zhong and my friends Yan Xue, Yu Sun, Jingqin Cui, Jinyong Bao, Yasumasa Ito, Xiaoxiao Chen, Bin Ren and Hsinyu Chen.

I own my deepest gratitude to my parents for supporting me throughout my studies. Thanks to my lovely husband Zheng for taking care of our baby Hector in the last two months and for providing a good environment in which to complete my writing up.

Lastly, I offer my regards and blessings to all of those who supported me in any respect during the completion of my Ph.D studies.

Contents

List of Tables and Figures

Chapter 1

Introduction

Introduction

The basic idea of our project is to build structures to mimic the cell membrane and microenvironment in order to embed active membrane proteins and study their effect on cell behavior. Supported lipid bilayers play a central role in the constitutents of such a biomimetic platform. We fused supported lipid bilayer on the surface of silica microspheres with different functional membrane proteins to perform different roles to fabricate specialized biomaterials with potential uses in high-throughput screening and biomaterials. In general, we called the self-assembled microspheres fused with supported lipid bilayer lipobeads (LBs). Furthermore, we applied transporter protein PDR5 and adhesion protein N-Cadherin into these systems, fabricated so called proteolipobeads (PLBs). Our research is focused on using a biomimetic approach to build a supporting structure with lateral mobility and functionality. The PLBs were synthesized with different membrane proteins and characterized by confocal microscopy and flow cytometry.

Molecular transporter proteins have extraordinary properties and are some of the most highly sophisticated molecules found in nature. These complexes bind and transport a variety of molecules and are considered "multidrug" or xenobiotic in nature[1]. In the cellular environment these proteins are responsible for removal of toxic metabolites via ATP-powered active transport against concentration gradients[2]. The systems in this class also provide the fundamental means for molecular transport for the cells, and are nature's smallest pumps, operating at a single molecule level[3]. Active transporters have been used by organisms as efflux pumps of therapeutic drugs and represent a major impediment to curative cancer chemotherapy and a leading mechanism for antibiotic resistance. Hence, they

represent a vast source of targets for drug discovery as these pumps must be thwarted via new drug combination therapies to reinstate the efficacy of current antibiotics and medicines[4].

There are specific challenges to overcome when working with these molecules. They require a stabilized, native biomembrane microenvironment in order to function. To study active transport mediated by these systems, the biomembranes must remain intact (intact lipid bilayer diffusion barrier). Lipid bilayers are self-assembled colloidal structures composed of lipid molecules. Lipid monomer's structure consists of a polar head group and a hydrophobic part consisting of two fatty acid chains[5]. In our study, we must preserve lateral mobility in addition to maintaining the membrane protein structure. The lipid bilayer will be anchored to the solid surface in some cases through polymer tethers in order to enhance biomembrane-to-surface spacing, the stability, and the mobility of lipid bilayers[6].

One of the applications of this work is to build an *in vitro* model of the PDR5 and other ABC multidrug transporters. When removed from the complex cellular environment, the PDR5 transporter protein can be studied without interference from the other multidrug transporters present. For example, in the yeast *S. cerevisiae* are over 12 distinct multi-drug transporters and can mediate a variety of cellular functions. The purification of PDR5 transporter plays an important role in building this *in vitro* model, and it becomes the preliminary task to approach[7]. These assemblies can be used to find new drugs that inhibit PDR5 transporter and could be used in combination therapy with other current antifungal drugs that have been neutralized by PDR5 drug efflux[2]. This approach can also be extended to the other transporters such as those found in multidrug resistance in cancer. In case of human cancers, mutations in PDR genes are often associated with MDR, because they

control the expression of individual drug pumps, some of which were shown to be members of ABC family of multidrug transporters.

Another application of supported biomembrane is to mimic cellular communication in the stem cell 3D scaffolds using the supported lipid bilayer assemblies. Human mesenchymal stem cells (hMSCs)-based therapy represents a growing interest by researchers in regenerative medicine and tissue engineering. There are lots of dissatisfactions with current treatments such as poor viability, lack of functional cells and low engraftment efficacy. A novel microencapsulation technique is introduced here as an effective cell delivery mode for clinical applications of hMSC-based therapy. We developed this cell delivery device to provide stable and injectable migration-supporting matrix to hMSCs, which may present optimal biological and functional profiles for clinical application of hMSC-based therapy. The 3D tissue engineering barrier addresses hypothetically so many concerns we would overcome: Can we develop a biomaterial to manipulate the control stem cell and tissue regeneration? Is that possible to build a 3D stem cell scaffold to study the cell-to-cell interactions by mimicking stem niche cells using PLB assemblies? The specific aim of this research is on building a platform to present laterally-mobille N-Cadherin fragments in PLBs to human mesenchymal stem cells in 3D culture. The PLB assemblies can be synthesized with various surface ligand distributions, characterized and subsequently purified via FACS. Furthermore, ligands found to influence stem cell behavior in 2D culture have been studied for decades and a multitude of important ligands have been identified. Yet, the essentially none of these ligands have been incorporated into 3D extracellular matrix scaffolds. Thus, our work provides a platform for exploring the function of ligands in stem cell

microenvironments (known as niches).

Background

Microsphere-supported membranes can be used to recreate a native-like microenvironment specific for the study of isolated individual membrane transport proteins[5] [8]. Interactions of the lateral surface of the membrane protein with neighboring lipid molecules of the bilayer can play a crucial role. Supported lipid membranes can preserve the lateral mobility of membrane proteins if the proper lipid composition is provided and the proteins do not interact unfavorably with the supporting substrate[9]. Some membrane proteins form multimeric complexes in their functionally active form. This requires the lateral movement that enables interactions with other molecules. Supported lipid membranes can preserve the mobility of the reconstituted protein, hence retaining its activity.

The characterization of transport membrane proteins has become a highly active research field as the antibiotic resistance problem has grown in proportion. One of the most frequently employed strategies in biological systems that demonstrate resistance to cytotoxic drugs is the efflux of these compounds from the cell via membrane proteins. There is a currently urgent need to understand and block the mechanisms that are involved in the efflux of drugs out of the cell[3]. Drug efflux is a major mechanism of resistance to drugs in both pathogenic microorganisms and cancer cells. The knowledge of structural and functional molecular characteristics of integral membrane proteins often requires their purification from native membranes[2]. In this chapter, the introduction of ABC transporters, lipid bilayer and liposomes, the purification strategies and the techniques of using CLSM to study the mechanism of transport membrane protein are discussed.

Transport membrane proteins are essential components of biological cell membranes. These proteins are responsible for active (ATP-powered) and passive molecular transport. The active transport procedure happens against the concentration gradient, which is driven by hydrolysis of ATP to form ADP. In contrast, passive transport occurs with the concentration gradient as such does not require an input of free energy. *In vivo*, transport membrane proteins responsible for multidrug resistance are found in the peripheral plasma membrane, a hydrophobic and a fluidic bilayer microenvironment necessary for maintaining the structure and thus functionality of these biomolecules.

Membrane proteins can be reconstituted in a functionally active form in liposomes, forming proteoliposomes. However, proteoliposomes are not stable under various processing conditions (e.g., shear stress, temperature etc.), limiting their use the construction of biomembrane assemblies for drug screening applications. Lipid membranes supported by solid surfaces of various topologies present a mechanism for enhancing stability under challenging flow and processing conditions. Supported lipid membranes that contain tethering to the substrate, due to an inherent supported structure, can have higher stability compared to proteoliposomes[10]. These materials provide a better choice for the reconstitution of membrane proteins for the development of novel materials.

Lipids and the Lipid bilayer

A lipid bilayer is a membrane or zone of a membrane composed of lipid molecules (usually called phospholipids), which is critical component of all biological membranes on earth [13]. The structure of bilayer lipid membranes can be divided into two important regions, the polar head region and the nonpolar tail region, shown in Figure 1-1. The polar head

is hydrophilic while the tail represents hydrophobic character [14]. Since lipid molecules contain regions that are both polar and nonpolar, they are called amphiphilic molecules. The bilayer is composed of two opposing layers of lipid molecules arranged so that their hydrocarbon tails face on another to form an oily core. Amphipathic nature of the lipid molecules causes them to self-assemble in aqueous environments in such a way that the hydrophobic tails are hidden from water. Due to their cylindrical shape, lipid monomers self assemble in a bilayer structure with the hydrophobic tails sandwiched between the polar head groups, which interact favorably with water molecules. But even this bilayered structure leaves the lipid tails exposed to water at the edges of the leaflet. This leads to spontaneous closure of phospholipids bilayer to form sealed compartments. In the case of two end chains, one of the tails is generally saturated while the other one is unsaturated with a double bond in the middle of the chain. Presence of unsaturation in the hydrocarbon tail affects the packing efficiency of the lipids and hence the gel to liquid crystalline phase transition temperature (T_g) of the assembled lipid bilayers [10, 15, 16].

Supported biomembranes

A number of studies have been interested in membrane-membrane interactions for understanding cellular surface characterizations. The researchers started to explore the use of planar supported membranes about two decades ago. Spherical structures were later introduced for forming supported membranes by using a tethering molecule at the end of polymer spacer, shown as figure 1-2. In this approach, a part of the polymer tether is integrated into the lower leaflet of the supported lipid bilayer (Figure 1-3), offers 4-5 times space for membrane protein to form proteolipobeads (PLBs). Reconstitution of

membrane proteins into lipid bilayer to form PLB is one of the most useful techniques to study the functional aspects of these proteins. The membrane protein or transport proteins were reconstituted with the artificial phospholipid bilayers[11, 12].

Liposomes and Proteoliposomes

Liposomes are fluid-filled pouch microspheres, whose walls are composed of one or several layers of phospholipids. There are three categories of liposomes, in which they have been divided based on size: Multilamellar vesicles (MLVs) are the biggest ones over 10,000 nm; large unilamellar vesicles (LUVs) with size from 50-10,000 nm and small unilamellar vesicles (SUVs) with 20-50 nm in size. Those liposomes were produced by different techniques including extrusion and sonication. The phospholipids are often isolated from cell membranes. This structure enables the liposome to encapsulate water-soluble compounds and help in the delivery of certain enzymes, nucleotides or drugs [17]. Liposomes are especially effective in treating diseases that affect the immune system, which make them a very interesting model for the study of molecular mechanisms in living systems.

For medical applications as drug carriers the liposomes can be the best membrane model and can also represent a system in which the liposomes are potential drug carriers. The common step of preparation methods consists in evaporation the organic solvent in which the lipids are generally dissolved and stored. There are two major steps in making liposomes from dried lipids, sonication and extrusion [18]. The dried lipids are dispersed in an aqueous buffer solution by using vortex mixing, which obtain vesicles of different size and structures, the multilamellar or oligolamellar vesicles and unilamellar vesicles. Followed by the extrusion step, which is a process multilamellar vesicles are structurally modified to give

unilamellar vesicles. Vesicles are physically extruded under pressure through polycarbonate filters containing pores of pre-determined pore sizes. The resulting lipid dispersion is a homogenous formulation consisting of unilamellar vesicles or liposomes [8] within a narrow distrubution of diameters as tuned by the pore size.

PDR5 transporter protein

PDR5 transporter belongs to the PDR subfamily, which is the largest among these clusters and the drug transporters of *S. cerevisiae*. PDR5 specifies a 160-kDa protein with a predicted duplicated six membrane-spanning domain and a repeated putative ATP binding domain. PDR5, as in pleiotropic drug resistance, is the most well-characterized drug transporter of *S. cerevisiae*. When overexpressed, the PDR5 transporter confers resistance to a number of unrelated drugs[2].

A physiological role of PDR5 in effluxing compounds has been confirmed on the growth-phase-dependent expression. The PDR5 expression shows the highest accumulations during the effluxing of intracellular cytotoxic metabolites that occurs in the log growth phase. Decottignies et al[19].observed that the distribution of PDR5 gene in *S. cerevisiae* cells reduced the exponential cell growth rate. They proved that the presence of PDR5 is important for cell growth and those transporters like PDR5 may expel intracellular toxic products accumulated during cell growth.

Drug efflux is a major mechanism of resistance to drugs in cancer cells and other microorganisms. The mechanism of efflux in yeast *S. cerevisiae* cells relies on proteins that derive their transport energy from the hydrolysis of ATP. All of the putative drug transporters have been expressed in a strain of *S. cerevisiae* that is hypersensitive to drugs. The

presence of a number of resistance pumps with a variety of substrates provides *S. cerevisiae* with the ability to pump out a wide range of substrates.

N-Cadherin cell adhesion protein

N-Cadherin, a cell-cell adhesion molecule, is considered and mediated by both cell-to-cell and cell-to-matrix interactions. N-Cadherin is expressed at high levels in condensing mesenchymal stem cells and essentially plays a functional role in the cellular condensation process that leads to cartilage formation. The essential role of cadherins in stem cell niche is illustrated by the cell to proteolipobeads interactions. The N-terminal homotypic binding domain of N-Cadherin is available as a Fc domain fusion protein with a hexahistidine purification tag along with antibodies. Among the various commercially available human recombinant cell surface ligands and their antibodies, N-Cadherin was chosen for the proof-or-concept study because this protein has been shown to be involved in the condensation of hMSCs in chondrogenesis. Also, the N-Cad-Fc-His_6 domain is crosslinked by cysteine disulfide bridges which gives rise to homodimeric (N-Cad-Fc-His_6)$_2$ binding capacity to Ni^{2+}-NTA-PE molecules in the lipid bilayer.

Artificial stem cell niches

Stem cells have been characterized by their widespread potential of self-renewal for regenerative medicine and stem cell based therapy for genetic disorders and cancer. Regeneration of stem cells is critical based on both their ability to reproduce themselves and their differentiation ability. To retain their unique functions, stem cells integrates their population with an instructive microenvironment, called stem cell niche. However, in order to understand stem cell behavior and their regulatory mechanisms, researchers have

been working on engineering some specific functional stem cell niches *in vitro*, which refer to the material technologies.

In our research, we fabricate the cell adhesion PLBs to mimic the stem cell microenviroments in the collagen matrix and create artificial stem cell niches and control the cell-to-cell interactions by displaying N-Cadherin within these systems. The hybrid scaffold with stem cell and artificial cells, termed N-Cadherin PLBs, when encapsulated within hydrogel matrices can be studied as artificial niches. This is termed biomimetic ligand display, providing stem cell substrates within the 3D microenvironment. There are three advantages of these biomimetic stem cell substrate, a) artificial niches offer low cost and simplicity, b) N-Cadherin PLBs provide three dimensional structures and a mobile lipid bilayer for lateral diffusion, c) PLBs can be characterized and sorted via FACS prior to delivery and d) PLBs could be used to display multiple molecules, which gives a new route to systems of high ligand display complexity.

Techniques

Fluoresence and Confocal laser scanning microscopy (CLSM)

The phenomenon of visible light photon emission by certain molecules when they are excited by absorption of incident radiation of suitable wavelength is called fluorescence. Fluorescence photon emission is caused by excited state to ground state electronic transition in a molecule after excitation with an incident photon. Due to a large amount of molecules in the condensed phase and lifetime broadening, a typical (organic) fluorescent molecule has an excitation and emission spectrum instead of unique line spectra. Due to the phenomena known as the Stokes shift, the emitted light is of a longer wavelengths than the absorbed

light.

Confocal microscopy, termed Confocal Laser Scanning Microscopy (CLSM), was developed during the last several decades and became the method of choice for obtaining clear 3D images of cells. 'Confocal' is defined as 'having the same focuses'. By illuminating and detecting from a single point in a specimen, the "pinhole" aperture of a confocal microscope filters out the incidental light from above or below this point of focus, which makes the focusing image very clear and sharp[20]. This technique enables control over the depth of field for imaging thick specimens and an ability to reject out of focus light to get sharply defined images (Figure 1-4). Key features of a laser scanning confocal microscope are the use of point-by-point scanning of the sample with an attenuated laser beam and the rejection of out of focus light through spatial filtering of the emitted light beam.

The confocal laser scanning microscope can be divided into four parts, the light source, the scanning unit, the photomultiplier and the multichannel detection. Schematic representation of the beam path for a confocal microscope is shown in figure 5. The light source is the illumination high intensity laser with a known wavelength. Incident light beam from the laser source is first attenuated through a narrow aperture called the source pinhole. Between laser and beam splitter, the excitation aperture produces a sufficiently tight (usually less than 0.2 micron) laser beam, which makes the scanning beam focus into the focal plane within the specimen. When fluorescence is excited, the exciting electromagnetic radiation is emitted in a spectrum of wavelengths know as an emission spectrum, giving rise to the specific color evidenced by the human eye.

The scanning unit provides the control of the laser illumination that allows for the

recording of the entire image XY plane at a fixed Z position. The traditional illumination system utilizes a series of lasers at different fixed wavelengths for fluorescence excitation. The sequential collection of light from wavelength filtered individual specimen points composes of the confocal images. These points are called voxels and their size is limited by several factors including optical resolution and the digital capabilities of the detection system. The point-by-point signals collection process requires a mechanism for scanning the focused illuminating beam through the specimen volume under observation. This mechanism is that the scanning unit writes the laser spot like moving a mirror that shifts the laser spot in the x-axis up to the end of a line, then on line down in the y-axis and again along the x-axis.

As to the photomultiplier, the user can control the intensity of images by increasing or decreasing the voltage of the photomultiplier by the computer controlling the CLSM. The aim of voltage changes is to produce an image with a pure black background and sufficient fluorescent signals.

After the collection of primary image information, the emission wavelengths of different fluorochromes can indirectly by analyze with muilti-channel detection by using several channels. In the simplest configuration each channel is provided with a fixed bandpass emission filter and a photomultiplier, which leads to the separation of different fluorochromes from each other and from the autofluorescence of the tissue and separately analysis of different colors. In spectral confocal imaging the emission spectra of each voxel is obtained in what is termed a lambda scan, in which imaging is in four dimensions, XYX and λ, the emission wavelength. In this mode of detection, each voxel is equivalent to a steady-state fluorescence experiment conducted at femtoliter-scale sample volumes.

Confocal microscopy offers several advantages. First major advantage is the controllable depth of field. Besides, the elimination of out-of-focus image provides the high resolution and contrast. Also, the ability to collect serial sections from thick specimens makes it the one of the most revolutionary advancements in the field of microscopic techniques. Another major advantage of the confocal systems is the ability to excite and detect multiple fluorescent probes simultaneously. This leads to the possibility of dynamic studies of multiple structures based on simultaneous multichannel, measurements of the distribution of specific labels on multiple molecules of interest [21].

Fluorescence Recovery After Photobleaching (FRAP)

Axelrod et al. developed the technique of fluorescence recovery after photobleaching (FPAP) to study the diffusive characteristics of biological molecules in living cells [22, 23]. The method relies on the ability to incorporate a fluorescent label into specific protein or lipid components. When an intense excitation beam focuses on a region of interest area in the cell, it bleaches the fluorescent molecules in the interested area on a short timescale (< 200 ms). If the recovery of fluorescence is monitor immediately in time after bleaching, the fluorescence recovery kinetics are measured. The analysis of FRAP provides the diffusion coefficient of the fluorescent molecule because the diffusion of the unbleached molecules into the illuminated region is measured [24]. A simulated recovery curve illustrating relevant parameters of a FRAP data shows in figure 1-5.

$$F(t) = \alpha F_p \sum_{n=0}^{\infty} [(\frac{(-K)^n}{n!}) \frac{1}{(1 + n(1 + \frac{2t}{\tau_D}))}] + (1 - \alpha) F_o$$

Where:

F(t) = Fluorescence intensity of the bleached spot at time t after bleaching

F_p = Prebleach intensity

F_o = Intensity immediately after bleaching

$\alpha = \frac{F_\infty - F_o}{F_p - F_o}$ Fraction of the mobile species

K = Parameter related to the degree of bleaching

$$\frac{F_o}{F_p} = \frac{(1 - e^{-K})}{K}$$

The τ_D parameter is related to Diffusion coefficient as

$D = \omega^2 / 4\tau_D$

This technique works on the two basic physical phenomena: 1) photobleaching, and 2) diffusion of fluorescent probes. The accurate analysis of FRAP data requires that the bleach event is essentially instantaneous, which means that it must be much shorter than recovery time. First, it is instructive to consider recovery times for different molecules using a typical beam radius of 1 μm, which leads to photobleaching of the molecules in that region. The second step is the bleach event happening in where one of more regions of interest is subjected to high laser illumination. Last step is the acquisition of a series of images after the bleaching at attenuated laser illumination. Analysis of fluorescence intensity recovery can give the parameters related to fluidity and mobility of the fluorescent molecules of interest. In common cases, the average recovery time for labeled lipid analogs within bilayers is from milliseconds to seconds, which makes the diffusion coefficient D=0.1-1$\mu m^2/s$. For proteolipobeads, which are membrane-embedded proteins in cells, The D value goes to 0.001-0.01 $\mu m^2/s$, corresponding to recovery times from seconds to tens of seconds.

Flow Cytometry and Fluorescent Activated Cell Sorting (FACS)

Flow cytometry provides a quantitative platform for the measurement of particle fluorescence. The particle could be cells or other microspheres with fluorescent labeling. The fundamental ability of flow cytometry is to measure the properties of individual particles[25]. A beam of laser light produces a single wavelength through each particle. Light scattering and fluorescence emission gives information about the properties of the particles. Light scattered in the forward direction is collected by a lens known as forward scatter channel (FSC) and the side scatter channel (SSC) measures the light at a 90^{o} angle to the excitation line, as shown in figure 1-6. FSC intensity gives the particle's size while SSC provides particle's information about granular content. Both FSC and SSC are unique for every single particle and can be used to determine different particle types in one heterogeneous sample.

The detector of flow cytometry uses separate fluorescence channels termed FL-1, FL-2, FL-3 and FL-4. Those optical filters block certain wavelength by absorption and let other light photons pass through. When light hits a photodetector, it generates a small current with associated voltage. This voltage is amplified by amplifiers and converted into electrical signals to generate plot graph. Different fluorescence labeling particle goes to different channel. Weak signals are expanded while strong signals are compressed by log amplification, resulting a distribution of "events" that are refer to the number of cells or particles.

The flow cytometer utilized in these studies is the BD FACSCalibur. One of the major applications of the BD FACSCalibur system is cell sorting. The term FACS comes from Fluorescent Activated Cell Sorting. By gating a specific region of interest, we can instuct

the sorter to eliminate the unwanted particles and purify the ones desired. In our study, the lipobeads have been gated according to their physical characteristics such as size by FSC and fluorescent signal. Ideally, the uniform lipid bilayer coverage will produce a single sharp peak in histogram of fluorescence channel. We sort out those high quality microspheres-supported lipobeads by FACS gating and eliminate the aggregated lipobeads as well as the lipobeads with damaged lipid bilayers.

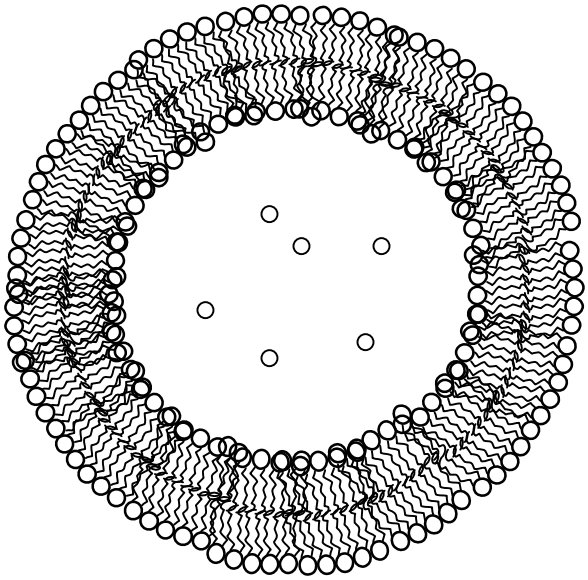

Figure 1-1. Schematic representation of phospholipids bilayer showing a encapsulated lipid vesicle separated from outside by a membrane barrier

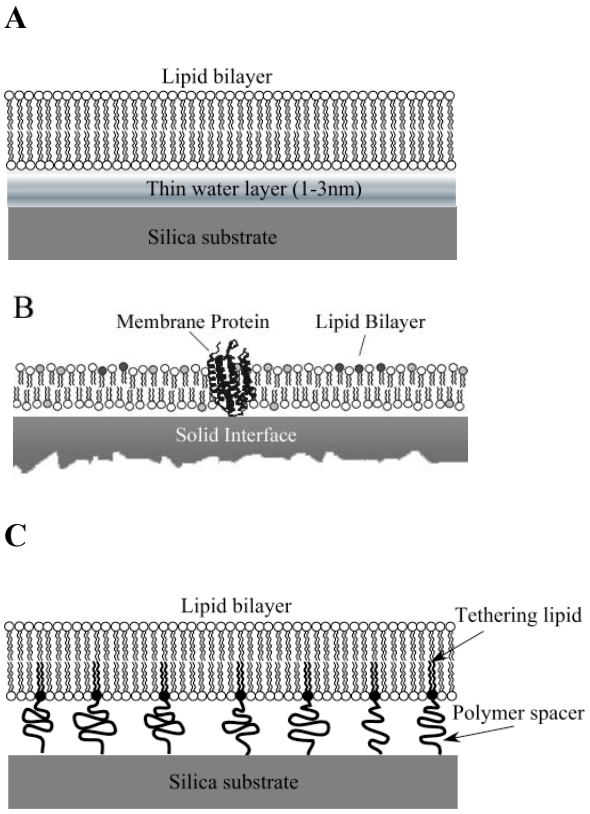

Figure 1-2. Various examples of surfaces of supported lipid bilayer, A) Free floating on a support, B) Membrane protein anchored on lipid bilayer, C) Tethered to the support through a polymer.

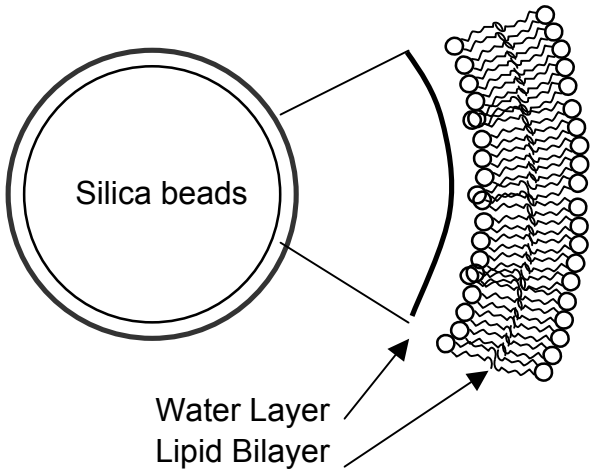

Figure 1-3. Schematic of solid supported lipid bilayer on silica microspheres

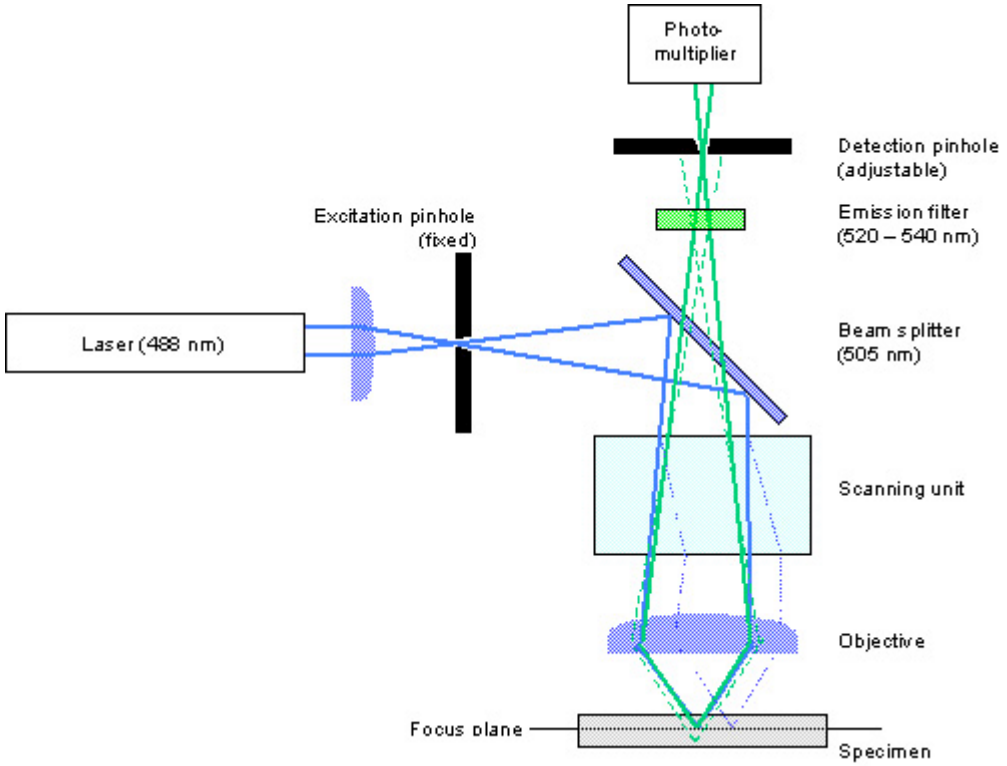

Figure 1-4. Schematic representation of the beam path in a confocal scanning laser microscope.. Excitation beam is attenuated by source pinhole, reflected by the dichroic mirror and is focused onto a small spot by the objective. Fluorescence generated from the excitation plane makes its way through the objective, dichroic mirror and detector pinhole into the photomultiplier detector. Fluorescence signal generated from the Out-of-Focus plane is rejected by the detector pinhole.

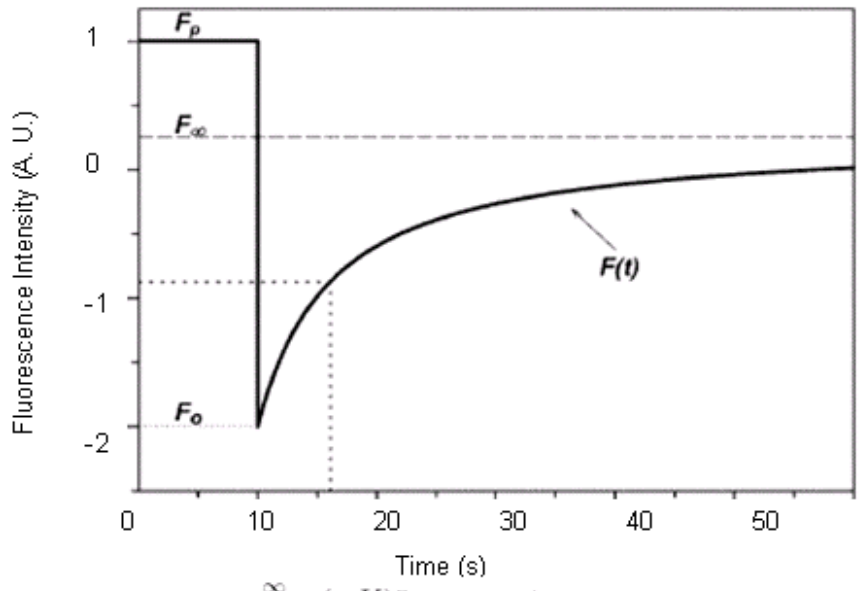

$$F(t) = \alpha F_p \sum_{n=0}^{\infty} [(\frac{(-K)^n}{n!}) \frac{1}{(1 + n(1 + \frac{2t}{\tau_D}))}] + (1 - \alpha) F_o$$

$$\alpha = \frac{F_\infty - F_o}{F_p - F_o} \qquad D = \omega 2 / 4\tau_D$$

Figure 1-5. A simulated recovery curve illustrating relevant parameters of a FRAP data. Schematic representation of a FRAP experiment showing the variation of fluorescence intensity of a region of interest (ROI) with time. Relevant parameters of the experiment have been shown. Also shown is the pulse sequence for the laser illumination intensity. A burst of laser intensity (~10X) for a short period of time leads to the bleach event. Postbleach detection is again done at attenuated laser power.

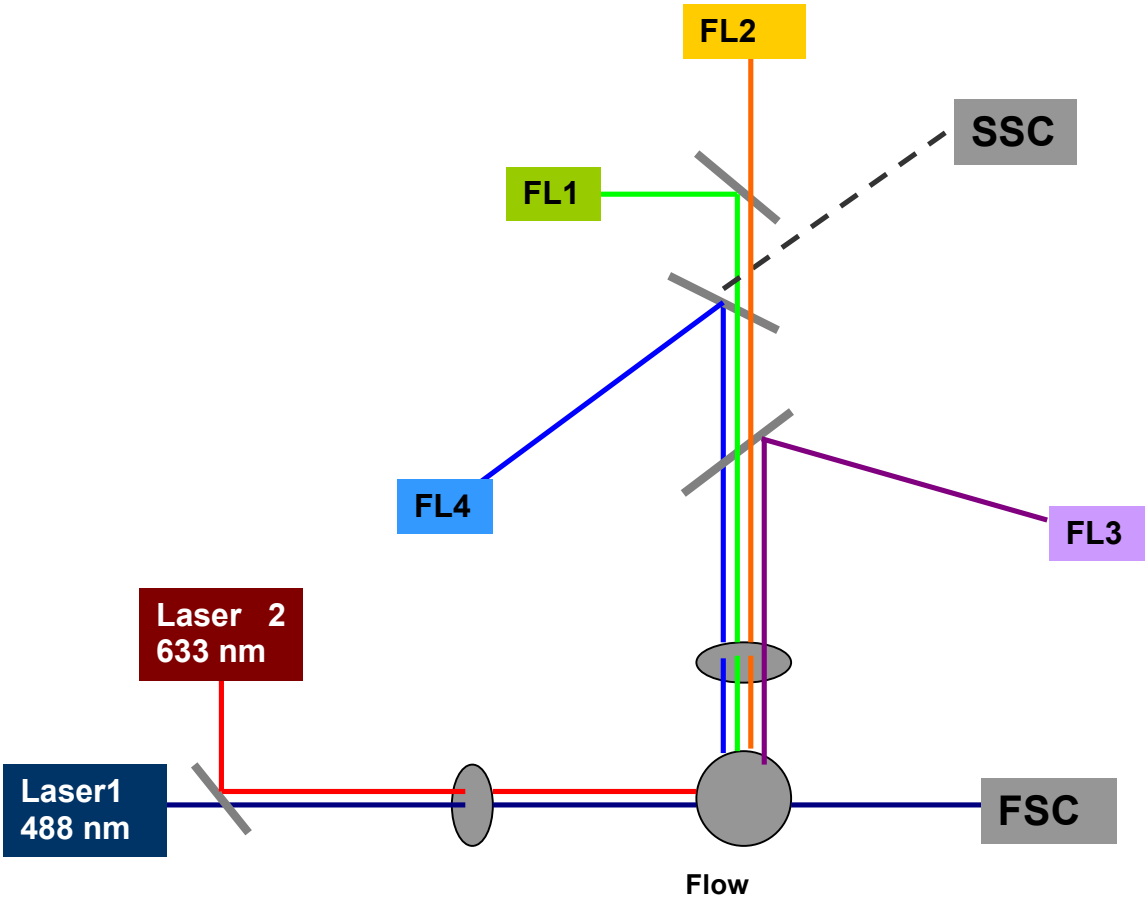

Figure 1-6. Schematic laser pathway of Flow cytometry of the BD FACScalibur System

FSC: forward scattering; SSC: Side Scattering

Chapter 2

Studies of the PDR5 pleiotropic drug resistance transporter protein of *S. cerevisiae*

Introduction

ATP-binding cassette transporters (called ABC transporters) contain two transmembrane domains and two nucleotide ATP-binding domains, which are the functional unit for transporting solutes across cellular membranes[7]. They help cells detoxify by continuously pumping deleterious molecules from the inside to outside of the cellular membrane. The hydrolysis of ATP functions as the energy provider for single molecule transfer against a concentration gradient, making the ABC transporter nature's smallest pump, a very unique nanomachine. Yeast ABC transporters comprise an extremely diverse class of membrane-transport proteins, which lead to the identification of 30 putative ABC proteins divided into six clusters, the PDR, MDR, MRP/CFTR, RL1, YEF3 and ALDP subfamilies. These subfamilies are shown in Table 2-1.

PDR5 transporter belongs to the PDR subfamily, which is the largest among these clusters and the drug transporters of *S. cerevisiae*. PDR5 specifies a 160-kDa protein with a predicted duplicated six membrane-spanning domain and a repeated putative ATP binding domain. PDR5, as pleiotropic drug resistance, is the well-characterized drug transporter of *S. cerevisiae*. When overexpressed, the PDR5 transporter confers resistance to a number of unrelated drugs[2].

A physiological role of PDR5 in effluxing compounds has been confirmed on the growth-phase-dependent expression. The PDR5 expression shows the highest accumulations during the effluxing of intracellular cytotoxic metabolites that occurs in the log growth phase. Decottignies et al[19].observed that the distribution of PDR5 gene in *S. cerevisiae* cells reduced the exponential cell growth rate. They proved that the presence of PDR5 is important for cell growth and those transporters like PDR5 may expel intracellular toxic products accumulated during cell growth.

Drug efflux is a major mechanism of resistance to drugs in cancer cells and other

microorganisms. The mechanism of efflux in yeast *S. cerevisiae* cells relies on proteins that derive their transport energy from the hydrolysis of ATP. All of the putative drug transporters have been expressed in a strain of *S. cerevisiae* that is hypersensitive to drugs. The presence of a number of resistance pumps with a variety of substrates provides *S. cerevisiae* with the ability to pump out a wide range of substrates.

Background

Separation science and technology is a very important area necessary for further developments in bio-oriented research and technology. Porous bead-based systems can provide a higher surface area for biochemical reactions than flat surfaces [26]. In the area of isolation or separation methods of bioscience and biotechnology, the beads can be trapped in microstucture using a magnetic field, a microchannel fluidic device, or used in traditional chromatography, ultrafiltration and precipitation procedures. The overall surface area of the beads can be coated by special ligands, chemicals, and binding biomolecules, which provide the support-to-target interactions that mediate the affinity purification [27]. In this project, both the magnetic separation method and affinity chromatographic system are based on polyclonal antibody interactions with the green fluorescent protein (GFP) fused to the C-terminus the transporter, which serves a dual role as a visualization marker as well.

The PDR5-GFP fusion protein target is shown schematically in Figure 2-1. This system was obtained by heterologous recombination [28]. GFP (Green Fluorescent Protein) is a protein first obtained from the jellyfish *Aequorea* that fluoresces in the lower green portion of the visible spectrum (emission maximum 509 nm). Fusion proteins of GFP have been inducted widely into living systems, providing detailed information about proteins dynamics and cellular localization. A number of transport protein-GFP fusions have been introduced into bacterial yeast and

mammalian cells, including the nefarious multidrug resistance efflux pump P-glycoprotein that confers taxol resistance to tumor cells in humans [29]. When the PDR5 transporters with GFP in the yeast *S. cerevisiae* growing in its log phase, the transporters fused to GFP protein emit intense fluorescent signals at the cell periphery, pumping the toxic materials from inside to outside of the cell membrane.

Magnetic affinity isolation

Magnetic affinity and ion-exchange separations have been successfully used in various areas, such as molecular biology, biochemistry, immunochemistry, enzymology, analytical chemistry and environment chemistry. Magnetism stands out as an interesting and important driving force to separate magnetic from non-magnetic components of the mixture when protein ligands are bound to magnetic particles[30]. Magnetic separation is usually very gentle to the target proteins or peptides[31]. Furthermore, even large protein complexes that tend to be broken up by traditional column chromatography techniques may remain intact when using the very gentle magnetic separation procedure [32]. Both the reduced shearing forces and the higher protein concentration throughout the isolation process positively influence the separation process. The mechanism is shown in Figure 2-2. Separation of target proteins using standard chromatography techniques often leads to the large volume of diluted protein solution. In this case, appropriate magnetic particles can be used for the concentration of the target molecule instead of adding ultrafiltration or precipitation steps to increase the concentration[33]. Evan GI and Lewis GK et al. use this magnetic method to isolate the monoclonal antibodies from human c-myc product [34]. Field J. and MacDonald B. also purified a RAS-responsive adenylyl cyclsae complex from *S. Cerevisiae* by use of this separation method [35].

Affinity chromatographic purification method

Bead affinity chromatography is a powerful method for purifying specific proteins from crude biological protein mixtures[36]. The target proteins are accumulated by an adsorption with ligand-binding beads and followed by an elution process. There are some difficulties in eluting the target protein in this micro-scale device. However, extremely high or low pH, a high salt concentration, detergents interference often cause the poor yields and result in a loss of functional target protein. The mechanism shows as Figure 2-3. The affinity coupling method has several advantages in practical experiments. It has been established and well-proven with high coupling success rate; Also it's suitable for immobilizing large proteins such as antibodies by coupling them to the matrix without the need for an intermediate spacer arm[37]; This affinity chromatographic method offers multi-point attachment resulting in a chemically stable product; Plus, the fast flow matrix gives high productivity and easy scale-up [38].

Materials and Methods

Yeast cell culture

Yeast cell disintegration buffer consists of 50mM sodium phosphate (pH 7.4), 1mM EDTA and 5% glycerol. Protease inhibitors buffer has to be freshly added into disintegration buffer to play its roles, which includes 1mM phenyl methyl sulgonyl fluoride (PMSF), 60 g/ml chymostatin, 5 g/ml leupeptin, and 7 g/ml pepstatin. Solubilization buffer contains 50 mM sodium phosphate, pH 7.4, 200mM NaCl, 1% n-dodecyl-β-D-maltoside, and freshly added protease inhibitors.

Strain: *Saccharomyces cerevisiae* YOR 153W (Invitrogen *S. Cerevisiae* Clone Library) Short-lived membrane ABC (ATP-binding cassette) transporter, actively exports various drugs, expression regulated PDR5; also involved in steroid transport, cation resistance, and cellular detoxification during exponential growth.

Culture medium: Rich medium Difco^{TM} YPD broth (Becton, Dickinson and Company), pH 6.50.1% NaN3 solution and 2% Glucose is applied after 7 hours inoculation to enhance the expression of PDR5 transporters.

Growth: 5-Liter Bioreactor is inoculated with 2.5×10^5 cells/ml for over 7 hours from an active preculture in small tubes overnight at 37°C. Yeast wet cell yields averaged 3 grams per liter.

Glycerol Frozen Stocks Preparation

Suspended yeast cells inoculated overnight are collected together and spin down at 4°C, 3000 rpm for 20 minutes. 20ml glycerol is autoclaved for 20 minutes and cooled down to room temperature. Four tubes, each containing 3.5 grams of wet yeast cells, are stocked by sterilized glycerol, which have to be made into 80 percent. With thoroughly mixed and divided into 1ml size small containers, the glycerol stocks are ready for freezing and later usage.

Yeast cells disruption and solubilization

There are numerous methods in cell wall/membrane disruption used in the sparation of proteins from yeasts. Possibly the most common method used for yeast membrane proteins is glass beads vortexing, where cells break open because of shear forces, grinding between beads, and collisions between beads. Another common method is ultrasonic disruption mediated by high frequency sound that is produced electronically and transported through a metallic tip to an appropriately concentrated cellular suspension. This method can uniformly homogenize the cells membrane by using high frequency sound, without destroying inner construction of whole cell. In this project, the biological ultrasonic homogenizer and glass bead vortexing with 400 micron glass beads were used in yeast cell disruption.

Ultrasonic homogenizer (*BioLogics, Inc.)* works as transforming line voltage to

high frequency 20 kHz electric energy. The vibration from the probe are coupled to and intensified the titanium tip. The working conditions are 3 ml yeast cells with medium, 30% power, 50% pulser for half an hour. To control local heating caused by high frequency around the titanium tip area, the ice-cold water incubation system was used.

Glass bead vortexing takes place at presence of 400 micron glass beads at the concentration 1 gram per gram wet cells. Five milliliter yeast cell suspension in yeast cell disintegration buffer was mixed with five gram ice-cold and acid-washed glass beads. The mixture was vortexed 20 times for 30 s each time with an interval of 30 s on ice in case to keep the temperature as low as it possible. This procedure was followed by centrifuged at 11,000×g for 30 minutes and filtered by 0.2 micron filter. Over 10 grams of cells could be easily processed at a time.

Solubilization of the crude membrane protein solution took place after spinning down and filtering, while right before the magnetic separation and affinity chromatography. The crude membrane protein solution contain copious amounts green fluorescent signals, which is the symbol that the crude PDR5-GFP is ready for solubilizing. The solubilized buffer is composed of 50 mM sodium phosphate, pH 7.4, 200mM NaCl, and most important detergent, 0.1% n-dodecyl-β-D-maltoside. By applying 20× stock solution 1 ml into 4 ml yeast cell suspension for an hour with occasionally mixing and stirring per 10 minutes, the solubilizing process has been accomplished.

Magnetic Isolation using μMAC column

PDR5 with GFP were separated by using μMACs epitope tag protein isolation kits (*MACs*). Anti-GFP microbeads are chosen for isolating whole green fluorescent protein (238-residue polypeptide). The microbeads bind specifically to the target protein, and the

strong magnetic field can easily be applied to separate the magnetically-labled proteins from the non-specific interacting molecules. The target GFP-PDR5 protein can be eluted with high purity by applying elution buffer, and the elute solution is then ready for SDS-PAGE analysis. By incubating 50 µl anti-GFP microbead solution into 1 ml solubilized PDR5-GFP membrane protein solution for half an hour on ice with occasionally vortex, The ligand-binding membrane protein solution runs through the magnetic column within a strong magnetic field, followed by the high pH elution with low pH buffer neutralizing.

Multi-scale affinity chromatography purification

Antibody-based affinity purification is responsible for the recombinant protein attached to the column during the bioselective adsorption process. Affinity chromatography separates molecules on specific binding of antibody to a solid matrix such as Sepharose CNBr active beads [39]. Antibody (IgG) is bound covalently to the CNBr active beads, which are loaded into a column, and the mixture of target protein and other substances is allowed to pass over the beads. The target proteins are bound to the specific antibodies, while all the other components can be washed away. The specific proteins are then eluted, typically by a huge shift of pH values from as low as 3 to greater than 11. Since the high binding capacity of antibody IgG, the antibodies bind stably under physiological conditions of pH value, temperature and salt concentration. In our current research, macroscale and microscale affinity chromatographic methods were developed to deal with different sample sizes. Macroscale chromatography has been used extensively for large volume samples and is ready for plenty of samples and ready for scale-up in pharmaceutical, while the microscale chromatographic setup provides more sensitive and higher efficiency in very small amounts of important membrane proteins at high concentrations such as those come from human cells or disease biopsy samples. The reaction of CNBr active beads

with protein is shown as follows.

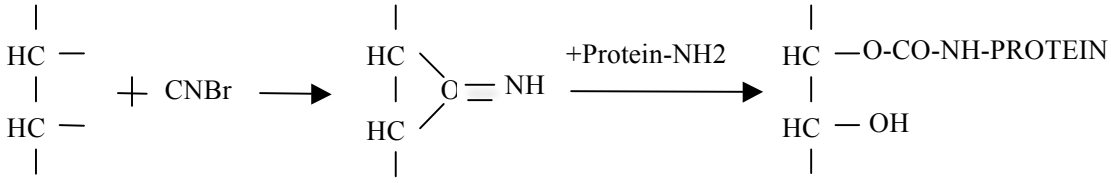

The macroscale GFP- based affinity chromatography setup is shown as follows. . Before loaded into the column, 500 mg sepharose CNBr-active beads were coating with 200ml IgG antibody overnight, the binding beads are called antiGFP-sepharose beads. We loaded 50ml antiGFP-sepharose beads on the column, with 50 ml crude detergent-solubilized PDR5-GFP biomembrane solution running through. The binding capacity of these beads is about 10-30 mg antiGFP per ml beads.

The microscale affinity chromatography device is developed with anti-GFP sepharose beads inside a microchannel chamber. The preparation of anti-GFP sepharose beads is the same as the macroscale one. Loading the anti-GFP sepharose beads is quite different from the column loading, a 3 ml syringe filled with 100 µl beads in 1mM Tris-HCl buffer has been used to load the beads.

Preparation for lipids and lipobeads

Lipid constituents were first dissolved in chloroform at 10mg/ml total lipid concentration. DMPC was the main constituent and was present in all the lipid formulations used. The T_g of DMPC is around 25˚C, which is above the room temperature. Therefore, the procedure of liposomes formation occurs at 30˚C water bath. Fluorescent lipid Texas Red-DMPC was also added to the chloroform solution at a ratio of 1:100 (probe:lipid). The lipid solution was then subdivided into parts containing 1 mg of total lipid stock and transferred into 4 ml glass vials. Chloroform solvent was evaporated using vacuum overnight or by a stream of N_2. Vials

containing lipid films were stored under argon at -20°C until required. To form multilamellar vesicles (MLVs), 1 mg lipid formulation was hydrated using phosphate buffer (pH 7.4) at 1 mg/ml and the suspension was subjected to 5 freeze-thaw cycles with vortexing in between cycles. Small unilamellar vesicles (SUVs) were formed by extruding MLVs through polycarbonate membranes (Avanti Mini-Extruder) or by sonicating the MLV suspension to optical clarity using tip sonicator (Biologics Inc. Ultrasonic Homogenizer, 150W model, microtip, 30% Power, 50% pulse, 15 min).

Result and Discussion

Dynamics of PDR5 expression in yeast cell growth

We have isolated PDR5 transporter protein as a GFP fusion from *Saccharomyces cerevisiae.* The GFP clone of S. cerevisae which produces this molecule is from Invitrogen. GFP fusion not only allows an intrinsic fluorescent label to track the protein during confocal microscopy imaging, but also gives a purification handle for using antibody-GFP during affinity isolation. PDR5 has been shown to be rapidly expressed in the cell periphery during the exponential growth phase. The PDR5 transporter exhibits transient expression relative to yeast cell growth. Displayed here in Figure 2-4 is the yeast growth curve as a semi-log plot of biomass concentration versus time. The cells were grown under aerobic conditions in a 5 liter bio-reactor using the classic yeast YPD media. Analysis of the GFP distribution showed that PDR5-GFP was located in the yeast plasma membrane during the exponential growth phase when the transporter mediates active transport of toxic metabolites. At around 6 hours after inoculation of the culture, we see PDR5 localized at the cell periphery in a confocal section. At stationary phase when growth slows and glucose is depleted, PDR5 expression is downregulated. The GFP fluorescence first accumulates in the cytoplasm in route to breakdown, as shown in the

confocal image taken at 12 hours. After longer time, such as overnight, there is very little GFP visible as shown in the image of the culture just after inoculation with stationary phase cells. This transient expression poses significant challenges in isolating PDR5-GFP.

Up-regulation of PDR5 in yeast cells

To solve this down regulation problem as mentioned above, we found a simplistic metabolic method to upregulate the PDR5. Transporter upregulation was carried out by incubating stationary phase yeast cells in 2% glucose under microaerobic conditions. To view the presence of glucose incubation over time, we immobilized log phase cells in an alginate gel. As shown the PDR5 upregulation and down regulation dynamics, the time scale of this transient behavior is about half an hour. This is the purification challenge: isolation of PDR5-GFP when the molecule remains present at high levels [40]. This transporter protein can be upregulated by either 2% glucose incubation for half hour or by exposing the cells to fluorescent probes such as rhodamine 6G. Figure 2-5 show the expression regulation of PDR5-GFP in real time under rhdamine 6G via CellASIC ONIX microfluidics system. Upregulation and downregulation are imaged by the series scanning of confocal microscopy on the order of minutes, complicating the purification process. The metabolic method can be applied in bioreactor. However, in order to image the yeast cell GFP expression under confocal microscopy, we have to get samples every ten minutes from the bioreactor and image it as soon as possible. To deal with this issue, another technology CellASIC has been introduced to upregulate the PDR5 expression. The core technology is the use of microfluidic methods to monitor living cells in real time via confocal microscopy time series scanning. We chose ONIX microfluidic perfusion system to obtain the upregulation control for yeast cells. The system integrates with CLSM to enable dynamic time-lapse experiments. A low-profile manifold connects the control system with the

microfluidic plates. The manifold forms an air tight seal using a vacuum mechanism. The wells of the microfluidic plate are addressed with pneumatic pressure to drive liquids into the microfluidic channels, preventing contamination and lengthy clean-up. The manifold and plate assembly fit into standard 96-well plate holders on confocal microscopes. The bottom imaging surface is #1.5 thickness glass slide, which is easily accessible by any objective lens. We obtained the 3D confocal microscopy images under series scanning mode. After introducing the Rhodamine 6G solution into the yeast culture medium, there is significant increase of fluorescence intensity at the periphery of cells.

The other challenge is the cells must be immobilized for imaging the distribution of the transporter. The alginate gel microenvironment traps the cells to enable confocal microscopy under static conditions so clear images can be obtained. Figure 2-6 shows a 3D reconstruction of the PDR5-GFP distribution in a representative yeast cell. The PDR5 is localized in high levels in the cell periphery, imaged while the live cell is conducting active transport of toxic metabolites. The pioneering proteomics work by Ghaemmaghami et al. with this GFP-fusion yeast library from which this strain was obtained, estimated that this transporter is present at levels near 42,000 molecules per cell [28]. From the standpoint of our proposed purification, in order to produce 10 micrograms of PDR5-GFP we would need to start with at least 1 gram of wet cells (assuming: d_{cell} = 10 mm; cell fraction = 50%; $Mw_{,PDR5\text{-}GFP}$ = 183 kDa)

We have begun to study the mobility of PDR5-GFP in cells relative to fluorescent lipids in supported membranes. Figure 2-7 displays representative FRAP data of PDR5-GFP in an immobilized cell versus that of a fluorescent lipid supported on a 5 μm silica microsphere (lipid images in inset). The lipid used was formulation 1 from table 2-2 doped β-BODIPY® 500/510 C_{12}-HPC with a molar ratio of 1:100 on a POPC basis. Analysis of these curves (as indicated in

chapter 2) gave values for the diffusion coefficient for PDR5-GFP as an order of magnitude slower than the much smaller and more mobile lipid, as expected ($D \cong 0.016\ \mu m^2/s$ versus $D \cong 0.75\ \mu m^2/s$ for the lipid). The fraction of mobile molecules within the bleached region was also lower for PDR5-GFP than for the lipid ($\alpha = 0.375$ versus $\alpha = 0.88$ for the lipid). These preliminary FRAP results set the stage for further studies with PDR5-GFP in supported membranes. As we have implemented this method to control the expression and begin to examine transporter mobility we next turn to the purification of the PDR5 transporter using affinity purification methods at multiple scales. The PDR5-GFP exhibited lateral mobility similar in magnitude to that found in the yeast cell, with much a greater fraction of mobile GFP containing protein in the supported membrane case.

GFP-based Magnetic Isolation

In this first type of purification, we tried (fluorescence) "exploratory" microgram scale using a magnetic affinity isolation method. We note that a microgram of GFP is a large amount of material from the standpoint of fluorescence as approximately 1000 molecules per individual voxel (250nm x 250nm x 400nm = $V_{voxel} = 2.5 \times 10^7\ nm^3$ = 25 attoliters) can be readily imaged, giving roughly 10 billion total voxels that could be imaged. This amounts to approximately 40,000 512x512 voxel images that each cover an area of 128 mm by 128 mm. However, the microgram scale is pushing the limits of many techniques used in the biochemical analysis of proteins.

First, we broke open the log phase cells using sonication in the present of protease inhibitors. This is followed by detergent solubilization and separation using anti-GFP magnetic nanobeads. Here we use GPF as the PDR5 purification handle. After elution from the column, we tested the sample with SDS-PAGE. The affinity purification gives a complex mixture

of peaks at high molecular weight, perhaps due to a complex mixture of fragments that includes multiple glycosylated forms. We were able to measure ATPase activity in the crude membranes using the Enzcheck assay from Molecular Probes. However we were unable to measure any activity from the purified PDR5. We attribute this either insufficient sample amounts (< 1 mg) or inactivity of the transporter in the sample. We ran the assay with PDR5-GFP in both detergent micelles and also after reconstitution into POPC-based liposomes using formulation formed from sonication. The detergent removal step in the reconstitution was accomplished by detergent dilution by a factor of 10. The total lipid weight was 100 mg; following the reconstitution the proteoliposomes were fused with 5 micron sized silica microspheres and rinsed to remove excess liposomes. We were able to detect PDR5-GFP supported biomembranes on 5 micron sized silica microspheres formed from proteoliposome fusion. We used spectral confocal detection to verify that GFP-PDR5 was present in the supported membrane, looking for microspheres that have supported membranes that exhibited emission spectra with maxima at 509 nm from the visualization reporter group GFP. In these samples only weak GFP signals were evidenced, in less than 1 out of 100 microspheres. For more comprehensive studies it is clear that a multifold scale-up of the purification was warranted.

Large-scale affinity chromatography purification

To go to higher purification levels we have implemented a high capacity porous bead affinity chromatography method based also on anti-GFP antibodies immobilized in 4% agarose beads. We chose to a commonly-employed 400 micron glass bead homogenization instead of sonication so that larger amount (> 10 g) of cells could be processed. The crude PDR5-GFP solution obtained gives copious GFP signals, as shown here using a handheld low power UV lamp. The confocal images from a Anti-GFP affinity purification from Yeast (top: Stage 1)

shows in Figure 2-8. We have been employing multiscale affinity purification routines including magnetic nanobeads (<1 mg scale) and AntiGFP-Sepharose porous beads in mini-columns (< 0.5 mg scale) and in microchannels (middle: Stage 2). The results of the characterization of the support are outlined as follows. The average diameter of anti-GFP beads was found to be 104 ± 19 μm. Analysis of microstructure of a GFP protein calibration standard within the beads via confocal microscopy gave a void fraction of approximately 0.45. Based on geometric arguments coupled to the analysis of GFP signal intensity we estimate that an averaged sized anti-GFP bead (d_{avg} = 104 μm) can bind ~0.2 ng of PDR5-GFP on the surface. Considering that the overall internal surface area is at least ten times this spherical surface area, borne out by measuring the fluorescence intensity fraction of the edge versus the inside of an equatorial section of a bead, this gives a maximum binding capacity of ~2 ng of PDR5-GFP per bead. The overall purification scale possible from loading 100 mL of beads (80% bed volume fraction ≅ 1,400,000 beads) is ~2.8 μg of PDR5-GFP. This figure is in rough agreement with the manufacturer's specification that the binding capacity of chymotrypsin was 1-3 mg per 100 mL of beads. A representative image (in equatorial confocal section) of PDR5-GFP inserted into the biomembrane on the silica microsphere via proteoliposome fusion is shown at the bottom of Figure 8 (Stage 3). This PDR5-GFP contained in this microsphere corresponds to approximately 0.5 attomoles (~85 femtograms; 170 kDa). Thus far we have been able to load only ~0.5% of the microspheres in a given sample with this level of PDR5-GFP.

We loaded the anti-GFP-sepharose beads with crude detergent solubilized PDR5-GFP biomembrane at 50 mL bead scale (diluted 5 fold from 10 mL concentrated bead stock), followed by pH 11.8 elution. Figure 2-9 displays the loading of the anti-GFP beads with GFP protein standard (0.02 mg/mL; Panel A) versus PDR5-GFP in detergent (panel B). The loaded

beads are both saturated with GFP and PDR5-GFP respectively at these conditions. Representative PDR5-GFP beads before and after elution are displayed in panel C. A dramatic reduction in intensity is evidenced upon elution. Analysis of a set of 8 beads before and after elution revealed that ~80% of the PDR5-GFP was eluted by the pH shift. Taking this into account we estimate that the scale of the purification has been brought up to the 10 µg scale.

SDS PAGE and Western Blotting

We loaded the elution solution in SDS PAGE gel and run an electrophoresis, followed by Western Blotting. A sharp single protein peak stained by Anti-GFP-HRP assigned tentatively to PDR5-GFP was observed after elution from the anti-GFP sepharose support (indicated by "*" Figure 2-10) with a line profile of scanned SDS PAGE gel. This yield is estimated at less than 10 ng PDR5-GFP/L. To further verify this finding we are starting to use dual affinity (N-terminus/C-terminus) purification scheme where GFP-containing (inactive) fragments (binding to Anti-GFP at their C-terminus) will not be captured in the N-terminus antibody binding step and are purified out.

Conclusion

In this chapter, we have shown the dynamics of yeast cell culture to express PDR5-GFP transporter protein. We have manipulated PDR5 up-regulation to achieve high expression levels of PDR5-GFP fusion using metabolic glucose trigger as well as fluorescent probe Rhodamine 6G. Preliminary FRAP experiments shows the lateral mobility in yeast cells and microsphere-supported lipobeads (PDR5-proteolipobeads). Multiscale purification were engaged in design the experiments in order to get enough material for further PDR5 proteolipobeads characterization. The yield is still in microgram level. However, we can still examine a sufficient number of microsphere assemblies to proceed and are currently engaged in the design and

implementation of single microsphere transport measurements adapted from bulk proteoliposome rhodamine transport assays. The preliminary low overall yields obtained from reconstitution into proteolipobeads precluded activity measurements due to the high detection limit of the colorimetric ATPase assay (2 mM). Further work is underway to increase the yields and produce PDR5 proteolipobeads with specific activities within those of published reports.

Table 2-1: ATPase Binding Cassette Transporters in the Yeast *S. cerevisiae*

Organism	Gene Name	Subfamily	Size	Function
Saccharomyces Cerevisiae	PDR5	PDR	1511	Drug efflux pump, phospholipid translocator
	PDR10	PDR	1564	Drug efflux pump
	PDR12	PDR	1511	Resistance to water-soluble, monocarboxylic acid with chain lengths from C-1 to C-7
	PDR15	PDR	1529	Potential drug tansporter
	PDR11	PDR	1411	Sterol transporter in anaerobic yeast
	SNQ2	PDR	1501	Durg efflux pump
	YCF1	MRP/CFTR	1515	Cd2+ and glutathione-S conjugate pump
	YOR1/YRS1	MRP/CFTR	1477	Oligomycin and multidrug resistance, phospholipid tranlocator
	STE6	MDR	1290	a-factor export
	BAT1		1559	Bile acid transporter
	ATM1	MDR	690	Mitochondrial DNA maintenance, essential protein
	MDL1	MDR	695	Peptide transporter
	MDL2/SSH1	MDR	812	Peptide transporter
	PXA1/SSH2/ PAL1	ALDP	870	β-oxidation of tatty acids
	PXA2/PAT1	ALDP	853	Interaction with PXA1, small-molecule

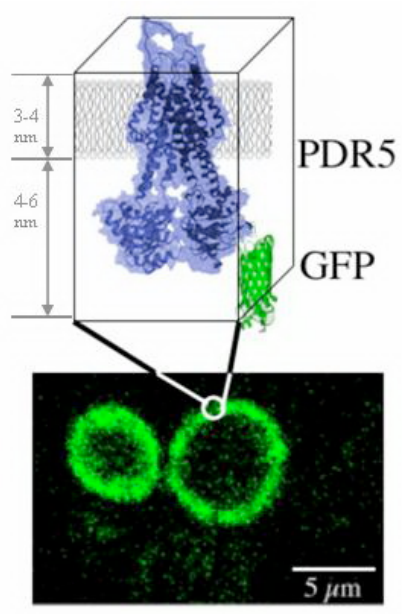

Figure 2-1. Schematic structure of PDR5-GFP fusion protein (top) and representative confocal microscope image of yeast cells

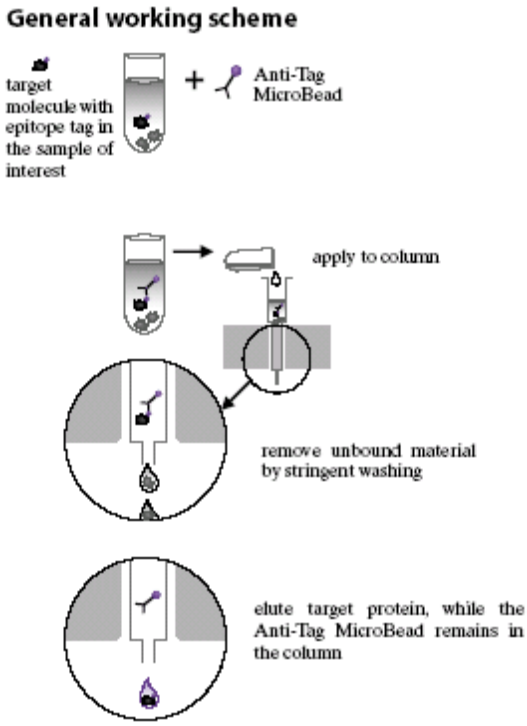

Figure 2-2. Mechanism of magnetic isolation. (General working scheme of μMAC)

1) Target molecules were mixed with anti-tag microbeads, 2) run the mixture through a magnetic column, 3) the anti-tag microbeads binding with target protein stays in the column, 4) elute target protein, while the anti-tag microbeads remains in the column.

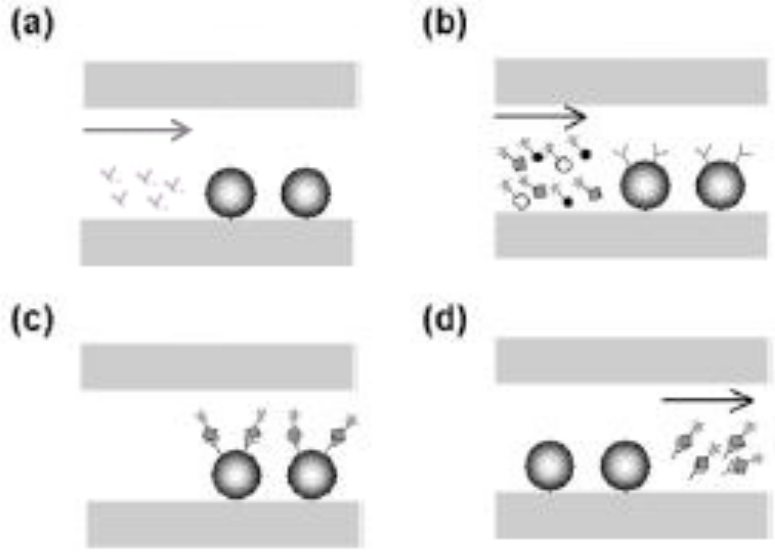

Figure 2-3. Mechanism of Affinity Separation Procedure. (a) Microfluidic antibody runs through sepharose beads, (b) Protein mixture flow runs through anti-GFP binding beads, (c) Target protein is bond to affinity ligand, (d) High pH and low pH elution

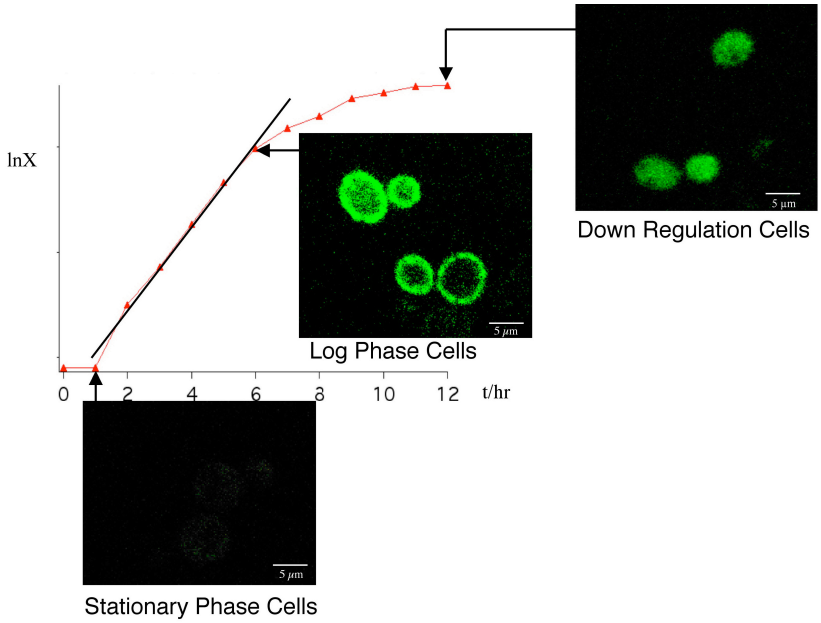

Figure 2-4. PDR5-Fusion protein target and confocal image of localization of PDR5 at the cell periphery

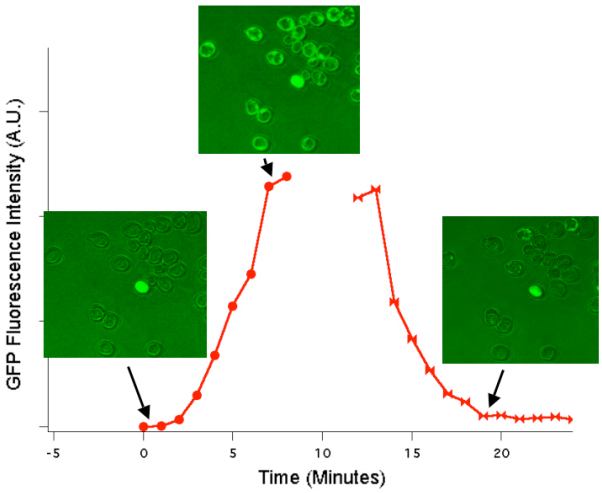

Figure 2-5. Expression regulation of PDR5-GFP under Rhodamine 6G addition and depletion in a CellASIC ONIX microfluidics cell physiology microdevice. Upregulation and down regulation occur on the order of minutes

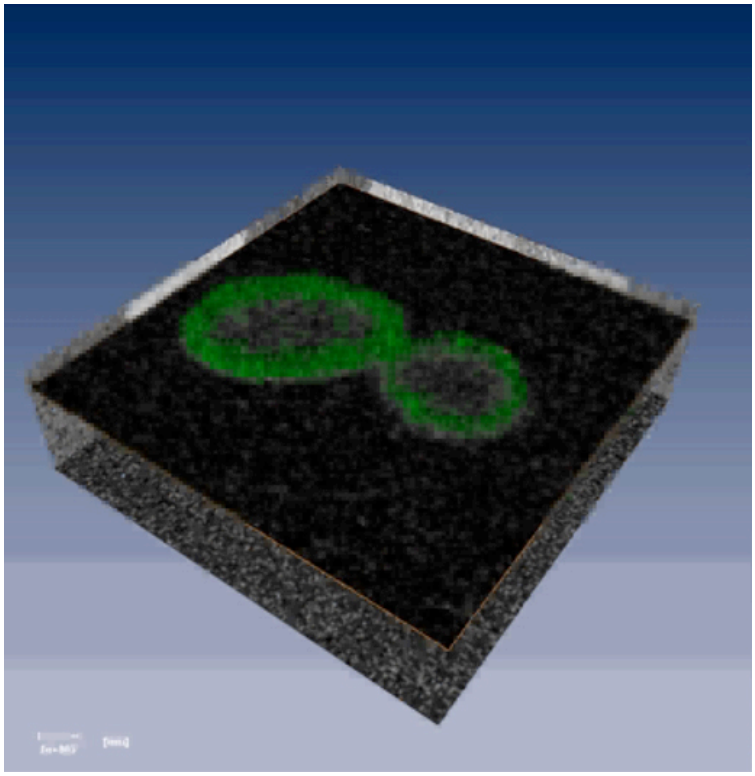

Figure 2-6. Localization of PDR5-GFP via Amira 3D image reconstruction

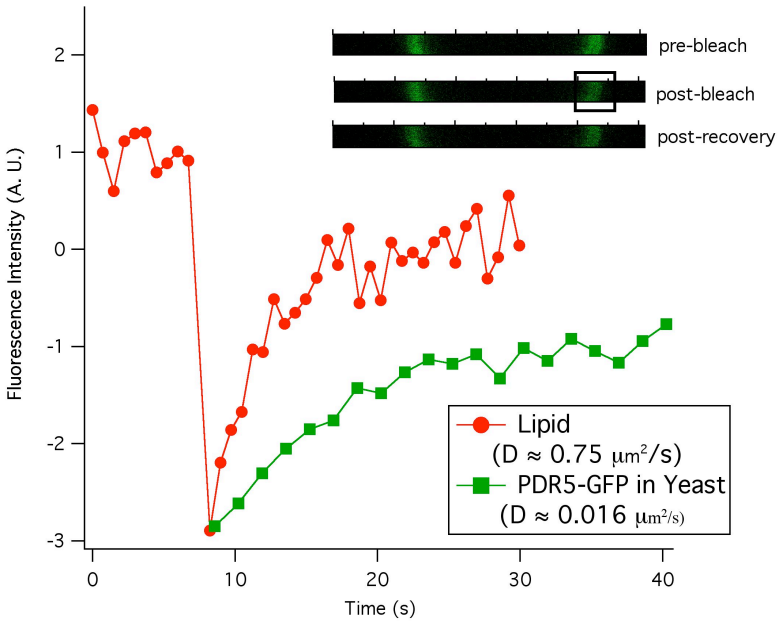

Figure 2-7. Preliminary Fluorecence Recovery After Photobleaching (FRAP) studies of fluorescent lipids in supported bilayers versus GFP-PDR5 in live yeast cells.

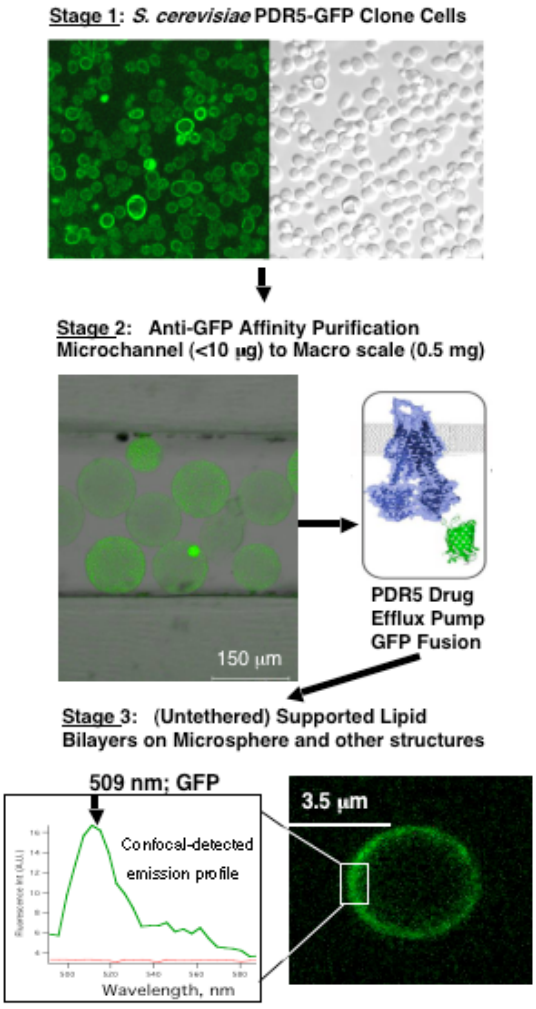

Figure 2-8. Confocal imaging of PDR5-GFP drug efflux pump in Yeast (stage 1), Anti GFP affinity purification via CNBR beads (stage 2), and GFP detected in a supported lipid bilayer via Confocal Microscopy wavelength scanning.

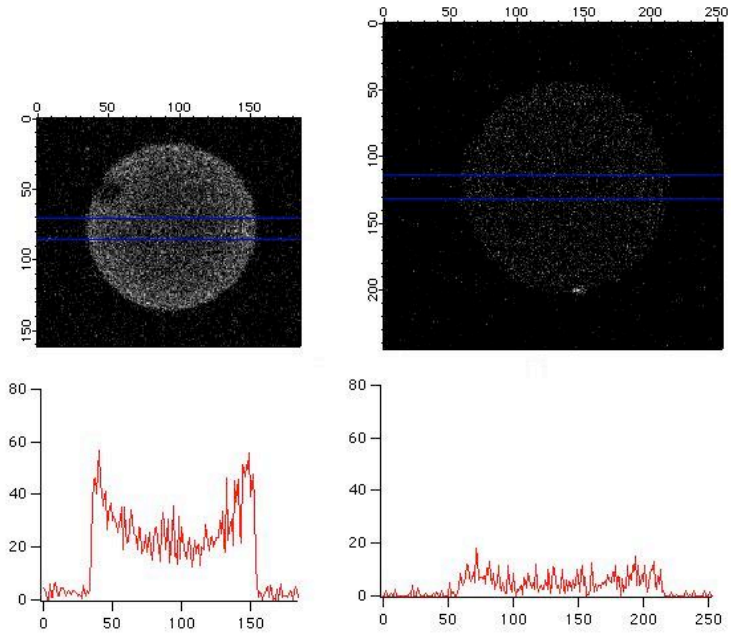

Figure 2-9. Image line profile of representative CNBr bead in anti-GFP-purification of PDR5-GFP Pre elution (Left), and after elution (Right) Fluorescence signal decreased ~ 80% by pH shift

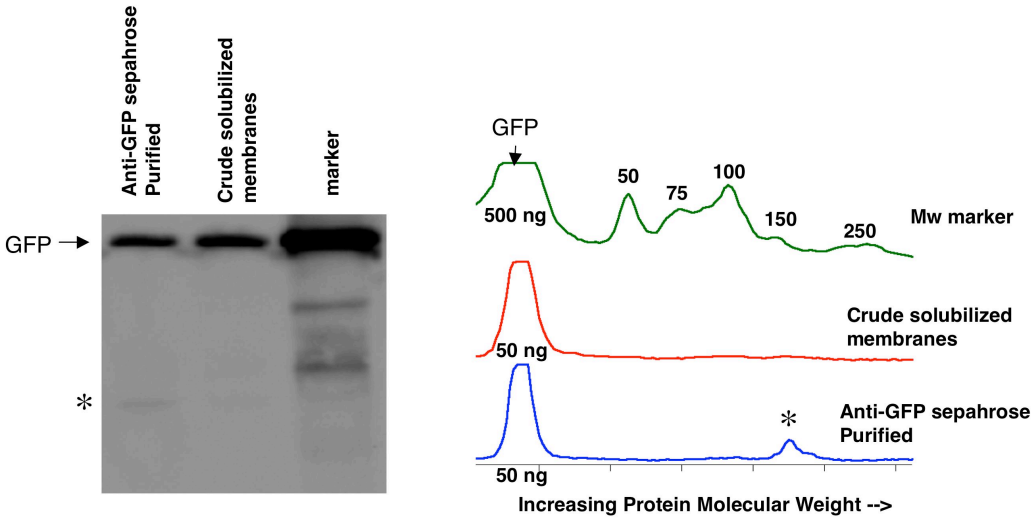

Figure 2-10. SDS-PAGE densitometry of GFP-PDR5 affinity purification. Western blot method with Anti-GFP-HRP/luminal chemiluminescence was used for gel imaging. The marker lane was loaded with 500 ng of GFP and the sample lanes were loaded with 50 ng each. Lane 1 was from the elution form the Anti-GFP-Sepharose support, Lane 2 was from the crude detergent solubilized membranes. A single high molecular weight band indicated by (*) is assigned to PDR5-GFP

Chapter 3

Synthesis and Characterization of Microsphere-Supported Lipid Bilayers (Lipobeads)

Introduction

Supported lipid bilayers have gained numerous attention due to their potential applicability in various areas[41] . They constitute a biomimetic platform for cell culture and a new approach to study the influence of membrane proteins on cell behavior. These systems serve a model of biological cell membranes for the design of biomimetic interfaces. Supported lipid bilayers can be functioned with bioactive molecules to increase specific cell adhesion. Also the fact that *in vivo*, lipid membranes house a variety of transmembrane proteins makes the supported membrane an ideal candidate for *ex vivo* reconstitution of these biomembranes upon isolation of membrane proteins from native cellular sources. Supported lipid bilayers are generally fabricated by the fusion and subsequent unrolling of lipid vesicles onto a suitable hydrophilic surface [42] [43]. The supporting surface could be modified silica, quartz, glass, and it can either be planar or spherical. A number of studies utilized lipid bilayers as model for biological cell membranes. Researchers have long been interested in studying membrane-membrane interactions for understanding cellular surface processes[44] [45]. Also the cell-to-cell adhesion studies have gained more and more importance in many fields. Furthermore, supported lipid bilayers exhibit low non-specific cell adhesion and protein adsorption from serum and cell media. Most commonly the planar format has been used in various studies. This was motivated from two underlying issues related to studying cell-to-cell interactions using micron-scale lipid vesicles as model for cell membranes. First, the effect of finite radius of curvature is difficult to take into account. And second, it's very difficult to observe the membrane-membrane contact using optical microscopy for both cell-to-cell interactions and cell-vesicle interactions[46].

In case of a lipid bilayer supported on a solid surface without any tethers, the membrane is separated from the interface by only a thin lubricating layer of water only 1-2 nm in

thickness. This water layer is sufficient to offer the lateral mobility to the lipid in the supported bilayer. Bilayers fabricated in the manner of polymer-cushioned layers or tethered to polymers can provide extra space for integral membrane protein to be reconstituted into the supported membrane and still keep their ability to diffuse laterally in the lipid bilayers. In the cases involving tether-supported membranes, a wide variety of tethering molecules have been employed ranging from polymers to peptides [47]. In our present research, our aim was to construct Biotin-PEG-PE conjugates and use them to anchor lipid bilayer membranes to streptavidin coated quantum dots and microspheres. This chapter describes the construction of biotin-PEG-PE conjugates for the formation of solid-supported membranes on particles. Also, the fabrication of PDR5 Proteolipobeads (PLBs) and N-Cadherin PLBs are discussed in our research (Figure 3-1.). We have used amine-based coupling to conjugate biotin-PEG-PE and those conjugates were characterized using FACS and CLSM. Streptavidin-quantum dot conjugates 525 and 655 were applied to facilitate the localization of biotin-PEG-PE and dye Texas Red was labeled to helping the fluorescence imaging via confocal microscopy.

One of the most widely utilized molecules in biotechnology is polyethyleneoxide-based polymer (otherwise known as poly (ethylene glycol): PEG or polyethylene oxide (PEO), which can provide a hydrophilic supporting surface for lipid bilayer. In addition, biotin-PEG need to be labeled by a fluorescent dye in order for us to localize it with confocal microscopy. PEG is a highly versatile polymer and a number of features such as biocompatibility and non-toxicity make it ideal molecules for in vivo applications. The highly hydrophilic characteristic offers modified surface to minimize protein adsorption. Furthermore, PEG can drastically modify its properties when conjugated to a protein. PEG modification shields the protein surface and can make it more water-soluble.

We have used different sizes of silica microspheres for tether supported beads. Silica beads were originally used as functionalizable surfaces for the design of liquid chromatography supports. p-Aminophenyltrimethoxysilane was used to modify the silica bead surface and form a self-assembled monolayer as it can give quite compact and uniform distribution of the desired amino functionality on the surface. This amine terminal functionality can be exploited further to attach molecules using N-hydroxylsuccinimide (NHS) based reagents. Di NHS PEG was highly reactive towards nucleophilic amine groups. The nucleophilic substitution reaction links the molecule of interest to the amines and liberates N-hydroxylsuccinimide as the leaving group. We explore the lipid bilayer on silica microspheres, functionalized with cell adhesion protein N-Cadherin, as substrates for cell-to-cell interaction.

Materials and methods

Materials

1-palmitoyl-2-oleoyl-sn-glycero-3-phosphatidylcholine(POPC),(Egg,Chicken)99%,1,2-Distearoyl-sn-Glycero-3-Phosphoethanolamine-N-[Amino(PolyethyleneGlycol)$_{2000}$] (AmmoniumSalt) NH_2-PEG-DSPE,1,2-Distearoyl-sn-Glycero-3-Phosphoethanolamine-N-[Biotinyl(PolyethyleneGlycol)$_{2000}$] (Biotin-PEG-DSPE) were purchased from Avanti Polar Lipids (Alabaster, AL) p- Aminophenyl trimethoxy-Silane 90% was obtained from Gwlest. Inc. No-Weigh NHS-PEO_4-Biotin was from PIERCE. Hydroxylamine. Quantum dots with emission maximums at 525nm, and 655nm. Deionized (DI) water. Phosphate Buffer (PBS pH 10), Tris-buffered Silane (TBS pH 7), 2-(4,4-difluoro-5,7-dimethyl-4-bora-3a,4a-diaza-s-indacene-3-pentanoyl)-1-hexadecanoyl-sn-glycero-3-phosphate, diammonium salt (BODIPY-FL C_5-HPA), Rhodamine-DSPE were purchased from Invitrogen.

Lipid bilayer Formulation

These formulations were mixed using chloroform and dried overnight under vacuum, forming a thin film in approximately 1 mg per vial. Structures are listed in Figure 3-2.

1) POPC/Cholesterol/BODIPY-FL C_5-HPA in 0.66: 0.33: 0.01 in molar proportions

2) POPC/Cholesterol/NH_2-PEG-DSPE/ Biotin-PEG-DSPE/Rhodamine-DSPE in 0.61: 0.31: 0.03: 0.03: 0.01 in molar proportions

Hydrophilic surface treatment of silica beads

We have synthesized microsphere-supported lipobeads at sizes ranging from 5-30 microns. 5 micron silica beads were commercial available with amine ligand, as well as 20 micron silica microspheres. While 30 micron porous silica beads have to be modified by the method of silanization [48], the most widely used method to derivatize silica surfaces. First, the 30 micron silica beads were weighed and washed in a 4% peroxide and 4% Ammonium hydroxide solution at 80-90°C for 10 minutes. The beads were then centrifuged and rinsed three times with deionized water and resuspended in a 4% peroxide and 0.4M HCl solution. This step was also performed under 80-90°C for 10 minutes followed by deionized water washing three times. Those beads were dried in the 50°C oven over night. We use Di NHS PEG crosslinking to activate amine-terminated surfaces with NHS. These surfaces are used to conjugate the amine-PEG DSPE lipids that anchor the biomembrane. We also have introduced membrane-lipid anchor-based bilayers. After the silica surface is modified by Di-NHS PEG, we use both Biotin-PEG-PE and Amine-PEG-PE to form the lipid bilayer. After biotinylation of the amine surface with NHS-PEO_4-Biotin, we can bridge with streptavidin to form a tethered bilayer. The tether linkage is PEO_4-Biotin: Streptavidin:Biotin-PEG-PE. We can use various fluorophore-labeled forms of streptavidin to aid in labeling sets of microspheres in encoding schemes.

Fluorescence labeling

Strepavidin conjugated Qd 525 and 655 were chosen to verify the Biotin-PEG-DSPE tethering. BODIPY-FL-HPC was applied as green lipid reporter fluorescent signal and Rhodamine-phosphaditylethanolamine (Rhodamine-PE) as red lipid reporter fluorescence in order to distinguish from one to another microsphere-supported biomembrane assemblies.

Results and discussion

We have fabricated microsphere-supported membrane assemblies using size 5 micron silica beads. Microsphere-supported lipobeads were characterized via flow cytometry and Confocal Laser Scanning Microscopy (CLSM). Figure 3-3 displays Fluorescence Activated Cell Sorting (FACS) detection and CLSM imaging applied to the purification of biomembrane-microsphere lipobeads. BODIPY-FL-HPC was chosen and shown in green color in CLSM imaging and detected by FACS using laser 488nm. Panel A is the acquisition density plot for a sample of lipobeads that had high heterogeneity in the sample. Each dot represents a measurement of a single lipobead in FACS detector. On the Y axis the side scattering intensity of the 488 nm laser line is obtained. This is plotted versus the fluorescence of each lipobead on the X axis. There are two grouping of lipobeads in the side scatter channel. The lipobeads that scatter at 200 are single particles, and higher order lipobeads, doublets, triplets and clusters have side scattering intensities at 600 units (doublets) and above (multiplets). A set of histogram of microsphere counts versus fluorescence intensity are displayed for the entire sample in panel B (top: blue histogram), as well as for to regions in which the lipobeads are sorted into separate CLSM imaging samples. Sorting regions R2 and R3 correspond to the middle and bottom cytofluorograms, respectively. These cytofluorograms are correlated with representative 3D reconstructions of the supported lipid bilayers on the biomembrane microspheres, displayed above and to the left of the traces. The unsorted 3D image shows a number of clusters and

multimers of lipobeads with low quality supported biomembranes, with the exception of the uniform and high-quality single lipobead at the top left of the image. For the case of the R2 sorting region mainly doublet supported membrane assemblies are evidenced (middle image). Sorting region R3 gave the best sample purification and single biomembrane-microsphere complexes with near uniform lipid bilayer coverage on each (bottom image). Panel C shows the increase in single microsphere percent biomembrane coverage (from equatorial Z sections) for the unsorted case versus the R3 region sorted case. The biomembrane coverage metric goes from 59% to over 95% with a dramatic tightening of the error bars that is indicative of a remarkable increase in microsphere quality has been gained by sorting. We will use this method with various fluorophores and to attempt to control all aspects of biomembrane-microsphere PLBs formation including PDR5-GFP and N-Cadherin loading, orientation and lipid coverage.

In order to study the fluidity of supported membranes, we have begun to introduce the AAO nanotubular filter joining with microsphere-supported membrane as a prototypical biomembrane fusion system. The nanotubular filter is composed of 200 nm diameter nanotubes (figure 3-4.) The experiment was designed by forming green fluorescent (BODIPY-FL) doped phospholipids within AAO filter nanotubes. Then this filter was positioned over a bed of PEG-tethered microsphere biomembranes labeled in red fluorescent (Rhodamine-PE) in a chambered cover slip (Nunc Lab-TEK II). A plastic tip fixed to a micromanipulator with 50 nm stepping in z direction was applied to bring down the equilibrium position of the filter slowly contacting with the tethered supported biomembrane microspheres. The fusion between red fluorescent and green fluorescent happened in the order of seconds. Further more, different size PEG-tethered microsphere biomembrane assemblies were introduced into this system. Figure 3-4C shows the 3D reconstruction of confocal scanning images of bigger beads and smaller beads. The one

with larger radius was able to contact the surface of AAO filter. Green fluorescent signals transferred from nanotubes to the microspheres due to the fluidity and mobility of tether-supported lipid bilayer. For comparison, two smaller beads that did not contact and fuse lipid bilayers to the filter retain their red fluorescence as Rhodamine-PE and did not give high levels of BODIPY-FL green fluorescence.

We also employed Quantum dots as streptavidin conjugated-quantum dots to track fluorescence in the tether-supported lipobeads system. Figure 3-5. shows the schematic structure (top) of Biotin-PEG tether supported membrane coated with Quantum dot 525nm and 655nm The surface of silica microsphere was modified by NHS-PEG_{3000}-NHS. Biomembrane template was shown homobifunctional crosslinking to amine-terminated surfaces, which offer greater spacing for lipid bilayer fusion to the surface of silica beads. The lipobeads were then modified by Biotin-PEG_{3000}-DSPE (2.5%) for streptavidin binding. Biomembrane imaged by binding of streptavidin-conjugated Qdots to Biotin-PEG_{3000}-DSPE within lipid bilayer was displayed here. The bottom panel gives CLSM wavelength scanning result, showing even distributions of streptavidin-Qd 525 and 655 emissions bound to biotin-PEG-PE on the the lipid bilayers of tether-supported lipobeads.

Sometimes the fluorescent signals are just adsorbed fluorescent probes immobilized on the surface of the microspheres that did not form supported lipid bilayers. To test for lateral mobility and fluidity consistent with lipid bilayers, confocal FRAP studies were conducted for both untethered lipobeads and PEG-tethered ones. Shown as Figure 3-6, a small region was bleached by high intensity laser light and the fluorescence recovery occurs in this region because of the lateral diffusion of lipid. The untethered lipid has a diffusion coefficient of 0.09±0.012 $\mu m^2/s$ and mobile fraction over 75.1±6.1 $\mu m^2/s$ while as to the PEG-tethered lipid, the diffusion

coefficient is down to 0.032±0.006 $\mu m^2/s$, and mobile fraction is only 66.2±4.9%. The tether-supported AAO filter has a diffusion coefficient of 0.015 ± 0.004 $\mu m^2/s$ and a mobile fraction of 51.3±9.2%. As we might expect, PEG tethering adds immobile lipid obstacles to diffusion in this system, however in all cases the presence of laterally mobile lipid bilayers was confirmed.

Conclusion

In this chapter, we have fabricated supported lipid bilayers in the forms of microsphere-supported biomembranes as well as AAO nanutubulous filter supported bilayers. We have given evidence of supported bilayer formation on microspheres and AAO filters through confocal imaging and FRAP studies. FACS analysis has been utilized for sorting out the high quality lipobeads with uniform lipid coverage. This technique can be used to characterize and purify the N-Cadherin proteolipobeads indicated in next chapter. Furthermore, we have employed Biotin-PEG anchor to modify the surface of silica microspheres in order to obtain greater space for different biomembrane proteins fusion. The preliminary CLSM imaging results have shown evidence for successful PEG tethering due to the Qd 525 and 655 streptavidin detection. FRAP technique has been applied for untethered lipobeads, PEG-tethering lipobeads and AAO filters. Hindered mobility was evidenced in lipid-tethered systems. Also, we have proved that AAO tubule to lipobeads fusion system gave evidence of lateral mobility of supported lipid bilayer.

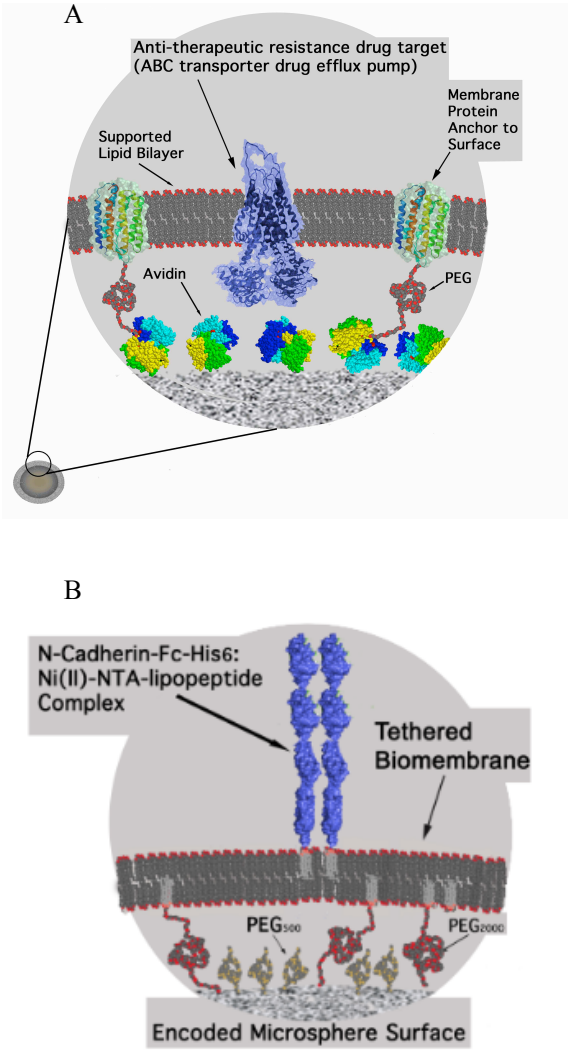

Figure 3-1. Schematic structures of PEG tethered PDR5 Proteolipobead (A), and N-Cadherin Proteolipobead (B)

POPC

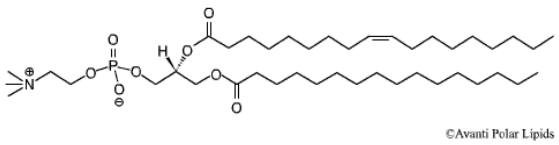

Cholesterol

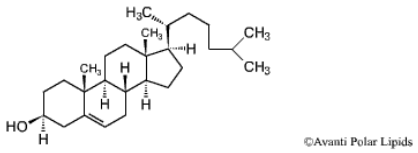

BODIPY-FL-PE

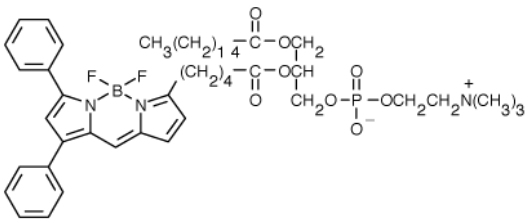

Di-NHS-PEG

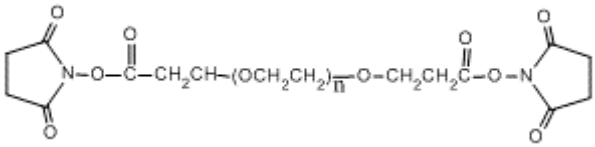

Rhodamine-PE

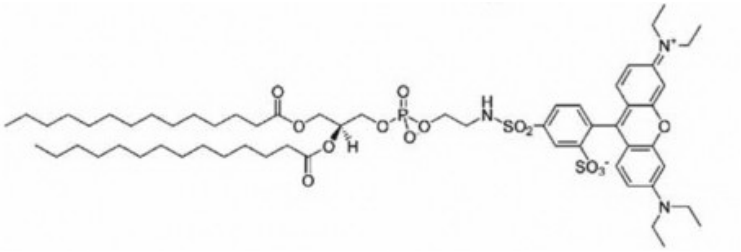

Biotin-PEG-DSPE

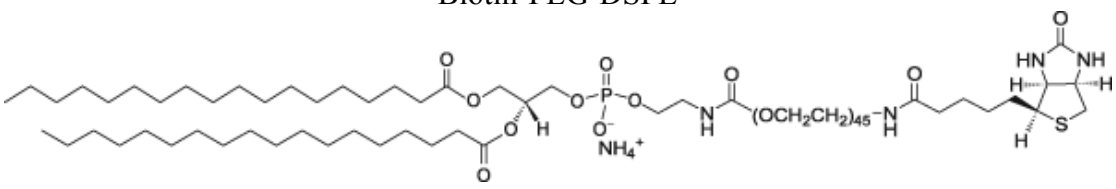

Figure 3-2. Structures of the lipid components used to make liposome formulations.

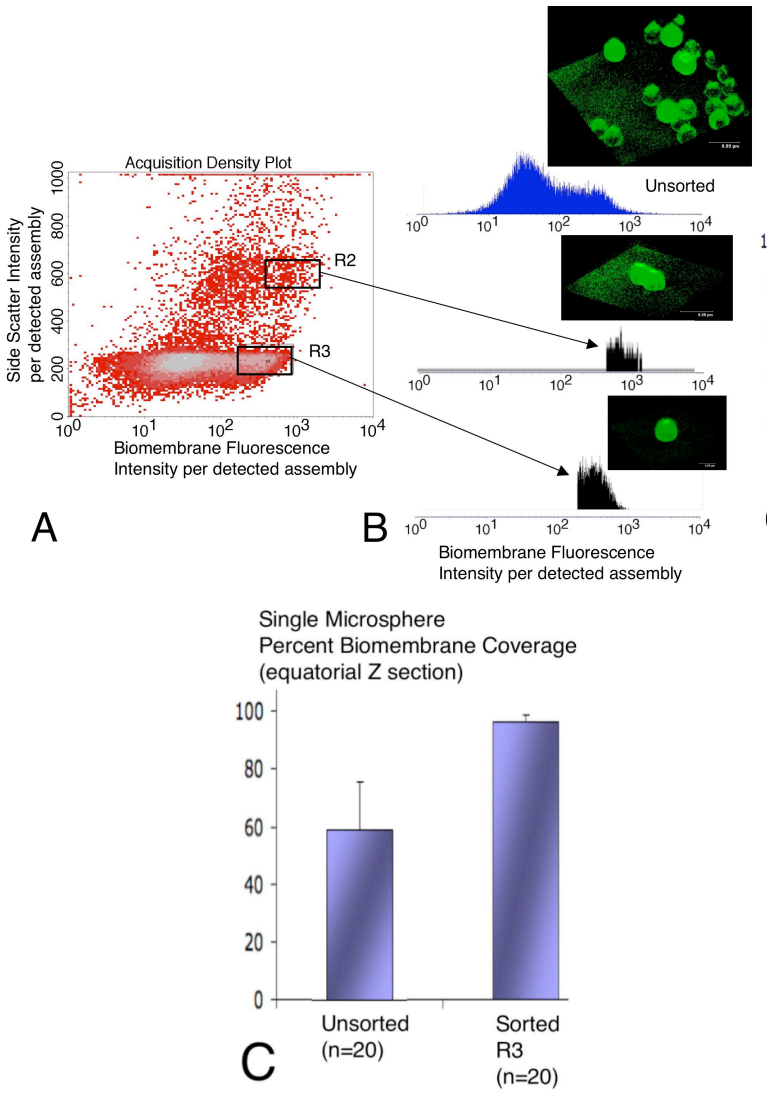

Figure 3-3. Fluorescence Activated Cell Sorting (FACS) applied to the purification of biomembrane-microsphere assemblies. Panel A is the acquisition density plot for a sample of biomembrane-microsphere assemblies with heterogeneity in the sample. Panel B a set of cytofluorograms (or histogram of microsphere counts versus fluorescence intensity) are displayed for the entire sample (top: blue histogram), as well as for to regions in which the assemblies are sorted into separate CLSM imaging samples. Sorting regions R2 and R3 correspond to the middle and bottom cytofluorograms, respectively. The

cytofluorograms are correlated with representative 3D reconstructions of the supported lipid bilayers on the biomembrane microsphere assemblies, displayed above and to the left of the traces. The biomembrane surface coverage metric goes from 59% to over 95% (Panel C).

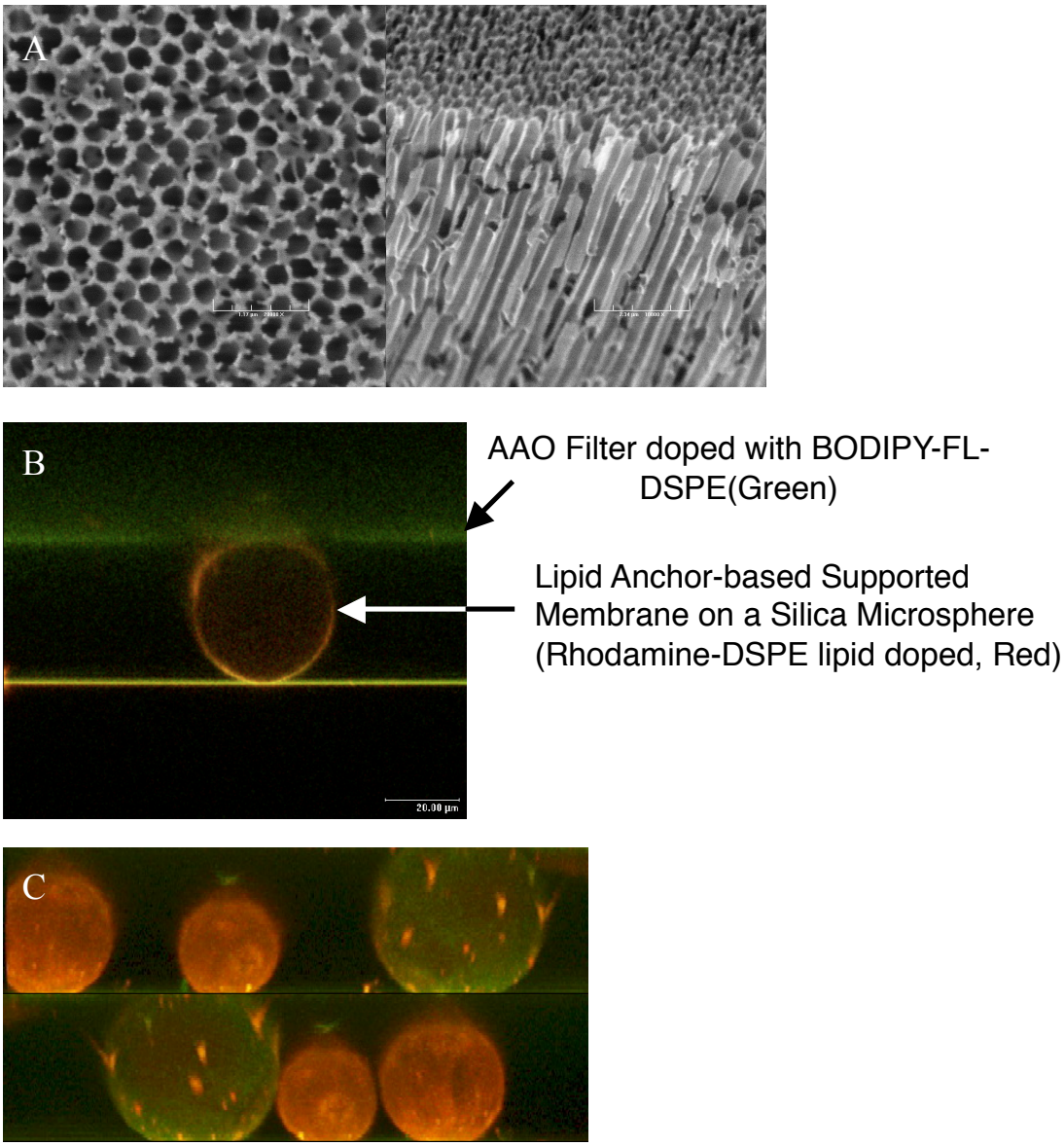

Figure 3-4. Fusion of nanoporous alumina lipid nanotubes with supported microsphere assemblies. A. Top view and side view of SEM image of AAO nanotubular filter. B. Side view of Confocal single scan image of fusion between AAO filter to Tether supported biomembrane on a silica beads. C. Two orthogonal views of the 3D confocal reconstruction of supported biomembrane on different size beads.

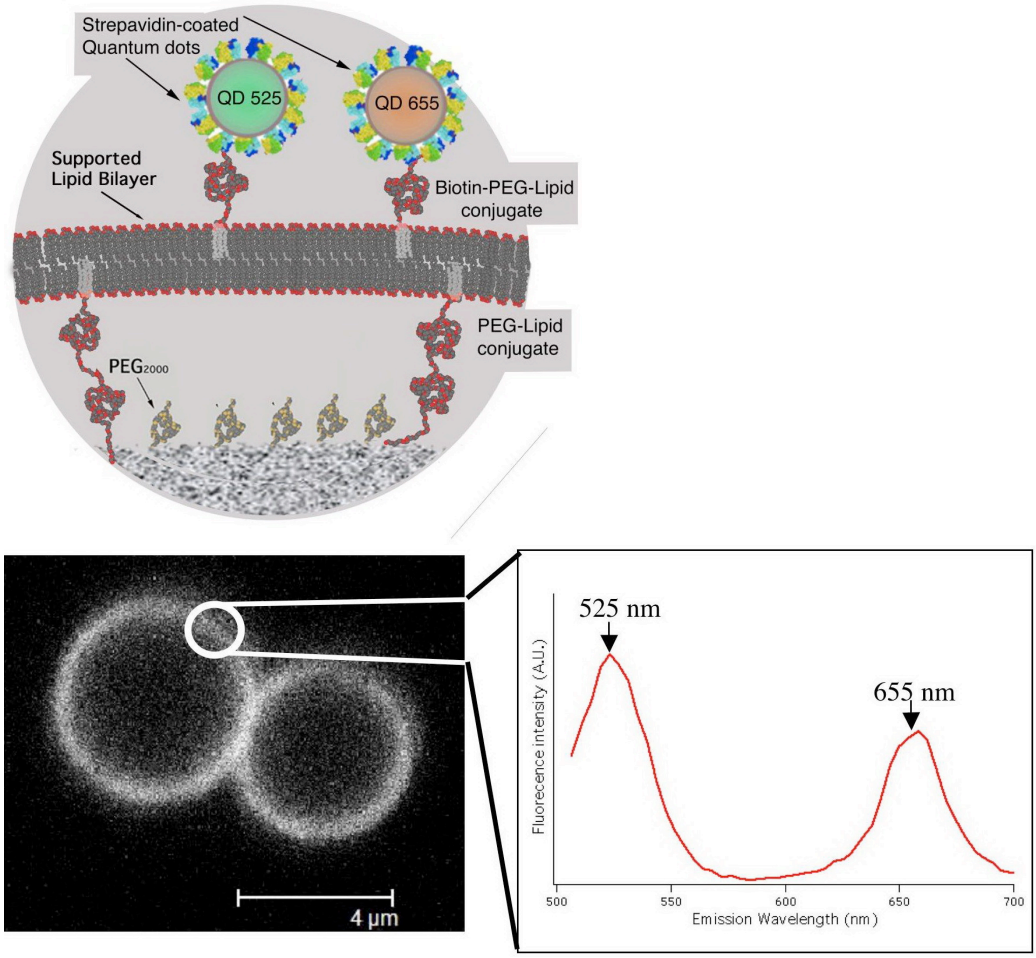

Figure 3-5. Spectral detection of streptavidin-quantum dot conjugates 525nm and 655nm on tether-supported Lipobeads (equatorial z section)

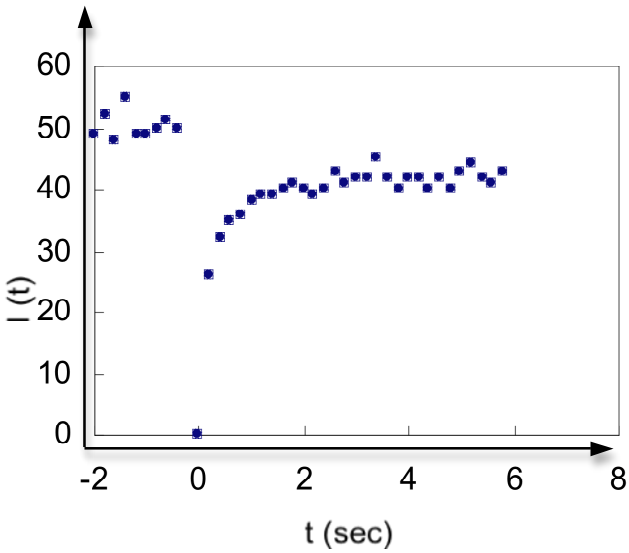

$$F(t) = \alpha F_p \sum_{n=0}^{\infty} [(\frac{(-K)^n}{n!}) \frac{1}{(1 + n(1 + \frac{2t}{\tau_D}))}] + (1 - \alpha) F_o$$

Where
F_p= Pre-bleach Intenstity
F_o = Intensity at t = 0 after photobleaching
α = Mobile fraction of the membrane

Type of support	Number of data sets	Diffusion coefficient (μm^2/sec)	Mobile fraction (%)
Silica-supported lipobeads	15	0.090±0.012	75.1±6.1
PEG-tethered lipobeads	15	0.032±0.006	66.2±4.9
PEG-tethered AAO filter	5	0.015 ± 0.004	51.3 ± 9.2

Figure 3-6. FRAP data analysis of silica supported biomembrane shown the diffusion coefficient and mobile fraction of silica supported lipobeads, PEG-Tethered lipobeads and PEG-tethered AAO filter.

Chapter 4.

New 3D Microenvironments for human mesenchymal stem cells via proteolipobead-matrix hybrid scaffolds

Introduction

Stem cells are characterized by their self-renewal capacity and the differentiation ability. [49]Controlling stem cell behavior outside of tissues will help understanding the stem cell mechanism without interference with stem cell's native complex microenvironment. Biomaterial technology could help create an artificial niche and engineer specific aspects of functional stem cell niches. Re-creation of the complex 3-D microenvironment of the stem cell niche in order to elicit regenerative control is one of the major challenges in biomaterials research[50]. The overall aim of our effort is to test the hypothesis that the introduction of biomembrane-microsphere assemblies into 3D scaffolds is a viable biomimetic means to present ligands/bound factors to stem cells and mimic cellular communication in the stem cell niche [51]. We have developed a new platform to present molecules to stem cells within a biomimetic architecture: as laterally-mobile molecules embedded in the context of a tailored biomembrane. The presentation of ligands/bound factors involved in cell-to-cell interactions (e.g. cadherin) has begun in 2D culture systems by surface patterning but has not yet been well established in 3D stem cell culture systems [52] [50] [53] [54].

Another potential application of this study is baseline immunophenotyping of hMSCs released from the 3D construct with N-acetyl cysteine cleavage of PEGSSDA[51]. Collagenase cleavage of collagen type I would be examined by FACS with a selected panel of surface markers designed to test cell lineage [55] [56] and with the marker types recently outlined by the International society of cellular therapy[57].

We present results on three aspects of this study: 1) the fabrication and characterization of functionalized microspheres that contain supported lipid bilayers; 2) the construction and characterization of collagen-I/microsphere hybrid scaffolds that integrate tether-

supported lipid bilayers on microspheres of various sizes and 3) preliminary studies of human MSCs microencapsulated into collagen-I/microsphere hybrid scaffolds.

Background

Adhesion protein N-Cadherin

In recent years, it has become clear that the function of adhesion molecules on the cell surface is essential regulated and governed by specific ligands [58]. Adhesive interactions are involved in the cell-membrane associate receptors and can provide critical information of microenvironmental conditions. N-Cadherin, a Ca (2+) dependent cell-cell adhesion molecule, is considered and mediated by both cell-to-cell and cell-to-matrix interactions. N-Cadherin is expressed at high levels in condensing mesenchyme stem cells and is essentially plays a functional role in the cellular condensation process that leads to cartilage formation [59]. The essential role of cadherins in stem cell niche is to be mimicked by cell to proteolipobead interactions we introduce using the hybrid scaffold method outlined in this chapter. The N-terminal homotypic binding domain of N-Cadherin is available as a Fc domain hexahistidine fusion protein (N-cadherin (Asp160 - Ala724)-Fc-His_6) along with antibodies [60]. Among the various commercially available human recombinant cell surface ligands and their antibodies, N-Cadherin was chosen because of it's role in the condensation of hMSCs in chondrogenesis [61] [62] [63]. Also, the N-Cadherin in this fusion protein is crosslinked by cysteine disulfide links, that give rise to strong (N-Cadherin-Fc-His_6)$_2$ bidentate binding mode to Ni^{2+}-NTA-PE molecules we have positioned in the supported lipid bilayer [64].

A few studies have investigated cell adhesion in fluid surfaces. We fabricate the proteolipobeads with N-Cadherin ligand to mimic the in vivo stem cell niche. The presentation of multiple ligands in fluid supported lipid bilayers allows for ligand diffusion to

complement the arrangement of cell-to-cell interaction, as well as cell-mediated ligand arrangement presented by the extracellular matrix [65]. Many classes of cellular adhesion molecules contribute to recognition and coexist on the cell surface. Adhesion between giant vesicles and supported bilayers decorated with E-Cadherin fragments was studies in a cellular systems by Brochard-Wyart et al [66]. Nagaoka et al have studied mouse E-Cadherin expressed as Fc fusion protein was immobilized on collagen and fibronectin surfaces [67]. Cadherin have been in a model for cell adhesion in 2D with adenocarcinoma cells. The important precedent of our work is the studies of micrsphere-immobilized dimmers of N-Cadherin-Fc chimeras conducted by Mege et al, showing that N-Cadherin-Fc retains functional properties of adhesion cadherins [60]. N-Cadherin has been reported as an important mediator of mesenchymal stem cell condensation [68]. Results from N-Cadherin transient expression studies conducted by Tuan and Delise proved that N-Cadherin function is required for chondrogenic differentiation by the specific mediation of cellular condensation [61] [62][69].

3D Scaffold versus 2D culture

Biomembrane surfaces coated with bioactive proteins or peptides in 2D stem cell culture have been well done in many studies [50] [53]. The mechanism for functionalization of active ligand on biomembrane surfaces has three advantages, simple adsorption, Fc-fusion protein domains mediation and hexahistidine tagged protein surface chelation. Normal cells in the human body experience a three-dimensional environment. That's why we create the collagen matrix scaffold for stem cells to be artificially surrounded by other cells, adhesion proteins and biomembranes. The 3D tissue engineering technological barrier lies in the various concerns. Can we build biomaterials suited to this task? Can we develop a relevant cell biology knowledge base and manipulate and control stem cell and tissue regeneration? The overall goal of our study is

to create a platform for presenting molecules to stem cells in 3D scaffolds. This technology could enable qualitative investigations of the microsphere-embedded molecules on stem cell fate within the 3D context, as well as allowing for the mimicry of cell-to-cell communication in biomaterials, as in the niche microenvironment, figure 4-1. This cellular "crosstalk" is of high importance with roles in cell polarization, quiescence, activation and proliferation.

Collagen matrix mimicking extracellular matrix (ECM)

Type I collagen matrix has been well established as the artificial extracellular matrix in order to study the cell interaction behavior regulated between cells and their extracellular matrices [70] [71] [72]. There are two advantages perform this biomaterial method to regulate cell-ECM crosstalk. First, this artificial model is expected to break down the complexity of enormous number of distinct interactions in natural tissue development[73] [74] [51]. Second, when isolated from the labor-intensive animal models, the time and cost of research in regulating cell fate process have been cut dramatically. Many types of 3D in vitro models have been successfully applied in mimicking the natural ECM components to identify the tissue developments and regeneration capabilities. The ECM scaffolds or stem cell niche formation in 3D experiments up-to-date are either reconstituted type I collagen gels or gels from reconstituted basement membrane. In our study, type I collagen gel was chosen to construct the 3D scaffolds with embedded hMSCs and proteolipobeads. The cell-to-ECM interactions are not the major concern in these biomaterial design experiments. The collagen type I matrices offer a three dimensional platform of suitable scaffold structures for cell-to-PLBs interaction study. Thus we selected mild crosslinking chemistries to build this system. Collagen type I is of those advantages as follows, highly hydrated material, biophysically functional fibrils, strongly resistant to non-specific protein adsorption and non-toxic crosslinking schemes are used for assembly.

Materials and methods

Materials

1-palmitoyl-2-oleoyl-sn-glycero-3-phosphatidylcholine (POPC), (Egg, Chicken) 99%, 1,2-di-(9Z-octadecenoyl)-*sn*-glycero-3-[(N-(5-amino-1-carboxypentyl) iminodiacetic acid)succinyl] (nickel salt) (Ni-NTA-PE) were purchased from Avanti Polar Lipids (Alabaster,AL).1,1'-dioctadecyl-3,3,3',3'-tetramethylindodicarbocyanine,4-chlorobenzenesulfonate Salt ('DiD'; $DiIC_{18}(5)$) was purchased from Invitrogen. The hMSC was a gift from Dr. Sihong Wang's lab (Biomedical Engineering Department, CCNY). The hMSC culture medium was composed from MSCBM basal medium 440 ml (stored at 4°C), SingleQuots Cryovials 1 ml, MSGS 60 ml, L-Glutamine and GA-1000 (stored at -20°C). Recombinant Human N-Cadherin Fc Chimera, monoclonal anti-human N-Cadherin Propeptide-Phycoerythrin (PE-conjugated antibody) and monoclonal Anti-human N-Cadherin Propeptide-Fluorescein (FITC-conjugated antibody) were obtained from R&D Systems. Rat-tail collagen type I was purchased from Becton Dickenson Lab.

N-Cadherin PLB synthesis

The lipid mixture was made of POPC, cholesterol and NiNTA-DSPE in different molar proportions. POPC/ Cholesterol /DiD in 0.8: 0.198: 0.002 in molar proportions, POPC/ Cholesterol/ NiNTA-DSPE/ DiD in 0.7: 0.198: 0.1: 0.002 in molar proportions and POPC/ Cholesterol/ NiNTA-DSPE/ DiD in 0.75: 0.198: 0.05: 0.002. These formulations were mixed using chloroform and dried overnight under vacuum, forming a thin film in approximately 2 mg per vial. 2ml PBS buffer was then introduced to make the lipids concentration 1 mg/ml and the vial vortexed for 1 min. The lipids were refrozen at -20°C solid and thaw in 4°C water before an intense 15 min probe sonication was conducted in icy water. 30 micron silica beads were

incubated by Ni-NTA-PE lipid for 30 minutes with occasionally stir. A lipid bilayer was formed as a thin membrane in fluidic form where the individual lipid molecules are constantly in motion around the 30 micron silica beads. This step was followed by three time rinses with PBA buffer to get rid of access lipid as background signals. Human N-Cadherin Fc was then introduced into the lipid bilayer system [75]. The transmembrane domain of N-Cadherin Fc was taken function in the lipid bilayer cytoskeleton of the lipid beads after an hour incubation at 4°C, which were finally fabricated into proteolipobeads. The extracellular domain of N-Cadherin stood out as the calcium-binding domains, which will perform functional cell-to-cell binding and interacting.

PLBs characterization via flow cytometry and confocal microscopy.

To test the N-Cadherin coverage of the proteolipobeads, we applied monoclonal anti-human N-Cadherin phycoerythrin and fluorecein separately. Anti-human N-Cadherin phycoerythrin gives red color in cofocal sequential 3D scanning, which helped us distinguish the live stem cell stain (green) and NiNTA-PE DiD lipid bilayer (blue). In order to determine the surface density of N-Cadherin on the proteolipo beads, Quantum FITC MESF premix kit was performed. Quantum FITC MESP premix kits are used in the quantitation of FITC fluorescence intensity in Molecules of Equivalent Soluble Fluorochrome (MESF) units (Bangs Laboratories). The kit allows the direct quantitation of the fluorescence intensity of a sample in terms of MESF units, which were converted from the flow cytometry results. FITC MESF kits were comprised of 5 populations of calibrated FITC fluorescent standards, 4 populations of different levels of FITC fluorescent microspheres and 1 blank population. The FITC MESF kits have excitation and emission spectra matching those proteolipobeads labeled with FITC. In our case of research, Anti N-Cadherin FITC allows us estimate the N-Cadherin binding density.

Fluorescence labeling

Dye choosen was DilC18(5) (DiD) has the excitation at 644 nm and emission at 665 nm, which is far away from the FITC antibody emission and also can be distinguished from the phycoerythrin-labeled antibody. This dye inserts spontaneously into the N-Cadherin membranes.

Cadherin-mediated adhesion to lipid bilayers. 10% NiNTA-PE were labeled and decorated with N-Cadherin-Fc-His_6. At the same time, a DiD labeled supported bilayer was generated with the biomembrane-microsphere assemblies using calcium-free buffer. The primary means for imaging N-Cadherin display was based on the antibodies conjugated with either FITC or Phycoerythrin. An overlapping approach will be sparsely label the N-Cadherin with fluorophores using standard amine-based bioconjugation methods and detect the ligand displays directly.

EDTA chelation

The Ni-NTA-PE lipid bilayer of the proteolipobeads were detected by the performance of EGFP-His_6. The density of His_6 binding ligands Ni-NTA-PE on the surfaces of the assemblies was assessed using EGFP-His6. The EGFP-His_6 shows green fluorescent signals with the presentation of Ni-NTA-PE lipid [76]. We use EDTA to remove the Ni ions and examine the non-specific dinding of EGFP-His_6 and NTA fragments. The lipid bilayers with EGFP-His6 were gently rinsed with a sufficient volume of 1mM EDTA solution. The incubation was in the dark for 30 minutes at room temperature. The tagged EGFP protein could be chelated on NTA containing membranes. In the absence of Nickel ion, almost no more green fluorescent signal was observed and there is no difference between the membrane and the background signal was detected.

N-Cadherin surface density and coverage

Quantification of biomembrane surface distribution of N-Cadherin was determined by using a combination of confocal microscopy and flow cytometry. Confocal microscopy performed

the essential role of 3D reconstruction of images, detecting the amount of fluorescent signals of anti-Cadherin Phycoerythrin. Phycoerythrin (red color) has an excitation and emission wavelength, 488nm and 578nm, which could be distinguished from live cell staining in green color and DiD Ni-NTA lipid in the color of blue. Sequential scanning methods were used to effectively eliminate crosstalk between green (ex. 488nm; em. 510-545 nm), red (ex. 543 nm; em. 560-610 nm), and blue channels (ex. 633 nm; em. 650-750 nm). FITC anti-Cadherin was used for FITC MESF kits to quantify the density of N-Cadherin coverage. Quantum FITC MESP premix kits are used in the quantitation of FITC fluorescence intensity in Molecules of Equivalent Soluble Fluorochrome (MESF) units. The kit allows the direct quantitation of the fluorescence intensity of a sample in terms of MESF units, which were converted from the flow cytometry results. FITC MESF kits were comprised of 5 populations of calibrated FITC fluorescent standards, 4 populations of different levels of FITC fluorescent microspheres and 1 blank population. The FITC MESF kits have excitation and emission spectra matching those proteolipobeads labeled with FITC. In our case, Anti N-Cadherin FITC allows us quantify the N-Cadherin level on the PLB surface.

hMSC culture and passaging

Preparation of media: MSCBM basal medium 440 ml (stored at 4°C), SingleQuots Cryovials 1 ml, MSGS 60 ml, L-Glutamine and GA-1000 (stored at -20°C).

(1) Decontaminate the external surfaces of MCGS bottle, SingleQuots Cryovials and the MSCBM bottle with 70% ethanol. (2) Open the bottle of MCGS and add the entire amount to the 440 ml MSCBM. (3) Open each cryovial of L-Glutamine and GA-1000 to MSCBM. (4) Mixed well and incubate the media at 37°C water bath.

Thawing of cells: The recommended seeding density of hMSCs is 5,000 to 6,000 cells per

cm^2. A 17.5 Flask is applied to 75,000 cells and 20 ml culture medium. Get cells cryovial out of liquid nitrogen or move them directly from –80°C refrigerator. Wipe cryovial with ethanol before opening. Briefly twist the cap to relieve pressure, then retighten. Quickly thaw the cryovial in a 37°C water bath. Watch the cryovial closely. Thawing is ready when the last ice melts and remove it from the water bath. (no longer than one and half minutes) Remove the cryovial immediately, wipe it dry and rinse it with 70% ethanol. A micropipet is applied to add 5 ml of temperature-equilibrated medium to the thawed cell suspension. Centrifuge at 150x g for 5 mins, not much cells were spinned down. Use 400x g for another 2 mins at room temperature. Resuspend the pellet in a minimum amount of medium by gently pipetting up and down. Add around 20 ml medium in to prepared flask and the cell suspension. Incubate at 37°C, 5% CO2 and 90% humidity incubator.

Quantitation-------Cell counting by hemocytometer: Typsinize a monolayer culture, prepare a slide and insert the cells into a hemocytometer chamber. Count the cells on the microscope and calculate cell concentration. Typsinize (0.25 mg/ml) the monolayer and resuspend in medium to give an estimated 1x 10^6 cells / ml (appoximately 2 ml for one N-75 flask)**;** Mix the suspension thoroughly to disperse the cells; Clean the surface of slide and hemocytometer with 70% alchohol, followed by dionized water. Prevent scratching the semisilvered surface. Dried by kimwipe.; Mix the cell sample thoroughly by pipetting and collect about 20 ml into the tip of a pipetter**;** Transfer the cell suspension immediately to the edge of the hemocytometer chamber. Do not overfill the chamber; Select four 4X4 objective. Count the cells lying within this 1 mm^2 area. Calculate the average of the four count------65. The number goes to the concentration of ~x 10^4 cells / ml, which is 6.5 x 10^5 cells / ml. Since we use 2 ml as the total volume, we could be able to get 1.3 x 10^6 cells in total.

Changing culture media and passaging cells: Draw off all supernatant with a pipette via vacuum. Wash gently with sterilized PBS buffer once to remove debris in flask. Add 2 ml trypsin into flask to cover the cell layer sufficiently. Incubate for 5 min (maximum) at 37°C, 5% CO2 and 90% humidity incubator. Tap and shake gently to release the monolayer of cells into suspension media. Add 10 ml fresh media and mix the cells thoroughly by pipetting up and down for several times. Followed by cell counting step. Write down the new passage number on each flask. Add 25ml fresh media and leave the flask on the bench with left and right movement, as cells begin to reattach the surface of flask with the new media.

Freezing and maintenance

Cells will be stored at -80°C for two week in freezing buffer, made of Fetal bovine serum (FBS) 90%, Dimethyl sulfoxide (DMSO) 10%. Liquid nitrogen was used for long-term maintenance over a month.

PLB-MSC Hybrid matrix construction and characterization

Rat-tail collagen type I was purchased from Becton Dickenson Lab with an original concentration of 5 mg/ml. Collagen was immediately neutralized by 10x PBS and 1N NaOH on ice and diluted into final concentration of 0.5 mg/ml. Before the hMSCs were loaded into this system, proteolipobeads were suspended into the collagen gel and mixed well. After mixing, transfer the solution immediately to 37°C incubator for 30-60 minutes to initiate polymerization of the collagen. 3D collagen matrix was imaged by scanning electron microscopy and confocal microscopy 3D reconstruction scanning.

MSC loading

Stem cells were suspended in medium with an original concentration of ~$5*10^6$ cells/ml, which were mixed with the neutralized collagen solution with final cell densities of ~$1*10^5$.

The cell mixture was dispensed as 2-5 uL droplets by thin needle glass syringe onto a collection platform of a sterilized non-adherent parafilm surface. The droplets formed solid gel microspheres after incubating at 37 °C water bath for 30-60 minutes, which were then gently flushed with full medium into a mini Petri dish with 0.15 mm cover slip located in the middle for later confocal microscope imaging.

CLSM Data Analysis of PLB-MSC interactions

CLSM sequential scanning was performed after two hours MSC loading into collagen matrix as day zero data and 24 hours as day one, 96 hours as day four. In sequential scan mode, green, red, and blue images were recorded line by line in a sequential order instead of acquiring them in simultaneously, effectively eliminating crosstalk or spectral bleedthough between channels. Confocal settings were designed to optimize performance and image quality of the 3D data sets. Reconstruction of confocal 3D scanning images showed cell-proteolipobeads interactions and the coverage of N-Cadherin was obtained by the surface area covered by the MSCs to the total proteolipobead surface area ratio.

Results and Discussion

We can use various fluorophore-labeled forms of streptavidin to aid in labeling sets of microspheres in encoding schemes based on size and fluorescent contents. Figure 4-2 shows the prototypical barcoded assemblies characterized and uniquely identified within 3D collagen-1 gels. Panel 2A is the flow cytometry characterization of the six barcodes based on streptavidin-Alexafluor633 and streptavidin-AlexaFluor514 labeling. Figure 2B displays a representative 3D reconstruction of tether-supported biomembrane-microsphere assemblies embedded in a collagen-I matrix obtained by confocal microscopy (0.5 mg/ml Collagen-I concentration). The collagen fibers (in grey) are imaged in confocal reflection mode, without the need for

fluorophore labeling. Five of the six barcodes are readily identified in the 3D reconstruction on the basis of their emission spectra and size, indicated by the white letter population designation (the others are redundant barcodes). The depth of the 3D image was 15 microns along the Z axis.

Figure 4-3 shows scanning electron microscopy image of microsphere-supported biomembrane in collagen I hybrid (A), SEM image of gross fibrils of collagen I matrix (B), Confocal reflection image of a representative stem cell in collagen fibril (Scale bar: 1 μm). The collapsed fiber network in the SEM image is caused by sample drying prior to imaging, confocal detected collagen-I fibers network retains the 3D structure encountered by cells.

At the onset of the experiment a subset of the constructs in culture were examined with CLSM under live-cell conditions. The 3D reconstructions of representative hMSCs in microsphere-collagen-I hybrid scaffolds were shown in figure 4-4. Panel A was taken 2 hours after cell seeding from the transmission channel in confocal microscopy. At this stage, minimal remodeling of the collagen matrix has occurred and prominent collagen fibrils form the scaffold matrix. Trypsined stem cells were still in round shape after two hours loading into the matrix. Proteolipobeads labeled with AlexaFluor 633, ALexaFluor514 and DiO were loaded within the reachable region of stem cells. Panel B was acquired 2 days after seeding. The stem cells were growing in the collagen matrix and formed the characteristic “spindle” shape of hMSCs. In this image the cell was stained with LIVE/DEAD (calcein AM/ethidium homodimer) and fixed in parafomaldehyde. At this stage the collagen nanofibers have been remodeled and the prominent nanofiber structures have morphed into finer structures that have less reflection contrast. The hMSC cell shown has interactions with 3 N-cadherin-biomembrane assemblies (shown by arrows), identified by their size and fluorescent characteristics as barcode “C’”. The assemblies were loaded with N-Cadherin-Fc-His_6, in complexes with the His_6 binding “receptor”

ligand Ni-NTA-PE. We have verified that the assemblies at the top and bottom still contain intact lipid bilayers at the microsphere surface, as shown in the inset where the equatorial Z section distribution of DiO fluorescence is homogeneous as seen in the assemblies prior to loading in the scaffold. We note that these biomembrane assemblies include surface to lipid bilayer tethering mediated by microsphere-PEO_4-biotin:streptavidin: biotin-PEG_{2000}-phophaditylethanolamine complex formation, enhancing the stability of the lipid bilayer. Also prominent in the 3D reconstruction is a C' barcode (2.8 um) that has been engulfed by the cell (middle arrow) This could suggest that there will likely be a microsphere diameter threshold that will be most well-suited for surface ligand display in 3D or other particle size dependent effects. This is to be expected as evidenced by the size effects in the multitude of cell growth studies in micropatterned regions in 2D. These PLBs might too small for mimicking the cell-cell interactions in studies of the interactions between cells and PLBs. To address this issue, we decided to instead use 20-30μm PLBs instead of 4.7 μm PLBs. The surface modification on 30 μm silica beads was discussed in previous chapter.

Figure 4-5A describes the characterization of ligand display on N-Cadherin PLBs. We choose silica beads without surface modification as negative control, as green bar (left), Ni^{2+}NTA-DGS PLBs not complexed with N-Cadherin-Fc-His_6 were displayed as positive control in blue bar (middle). The red bar (right) is from N-Cadherin-Fc-His_6-Ni^{2+}NTA-DGS PLBs. All we incubated first in 0.1% BSA blocking and then at >2-fold excess Anti-N-Cadherin-FITC concentration, incubating at 4 C overnight. To analyze N-Cadherin coverage on PLBs, we applied anti-human N-Cadherin fluorecein to the bare beads (green column), the lipid bilayer fused beads (blue column) and N-Cadherin PLBs (red column) in this chart. FITC MESF kit was addressed to quantify N-Cadherin coverage on microspheres. The left axis is given in

Molecular Equivalents of Soluble Fluorescence per PLB, obtained from fluorescein calibration beads from Bangs Laboratories run at the same settings. The detected N-cadherin displayed per PLB is 10 fold greater in the N-Cadherin PLBs (red bar) than in the case of the negative controls (green and blue bars)

To further analyze ligand display within the scaffold we constructed the microsphere/collagen I matrix without interference of stem cells to analyze the N-Cadherin ligand distributions on the proteolipobeads. Figure 4-5B is a composite 3D reconstruction of displayed N-Cadherin on a representative proteolipobead detected by Anti-N-Cad-FITC (green) within a collagen-I matrix (grey: reflection confocal imaging). The negative control sample with no added N-Cadherin-Fc-His_6 showed negligible signal levels at the same detector settings (data not shown). The average percent coverage was estimated as 80.2±8%, obtained form the equatorial Z section of a sample of 10 randomly-selected PLBs.

Figure 4-6 shows live and dead cell stain 2 hours after cell seeding (Day 0), and 24 hours after seeding (Day 1) and cell viability chart in, day 1, day 4 and day 7 with 30 micron PLBs loaded into the collagen matrix. We observe that MSCs start to interact with the PLBs as well as bind to the collagen type I fibrils. Both live and dead cells were found initially on day 0 culture. At day 1, considered the most important time frame of the relevance of PLB-to-cell interactions, high cell viability was evidenced. Numerous cell-to-PLB interactions were found in the collagen-cell-PLB hybrid system at day 1, we described these interactions further below.

3D CLSM reconstruction of hMSCs embedded in PLB/Collagen-I matrix were shown in figure 4-7 (Day 1 of culture). Collagen fibrils were displayed as white color, and N-Cadherin PLBs were in blue, as DiD lipid fluorescence. hMSCs were stained by calein AM in green. The upper left inset is at 63X magnification with collagen fibrils shown, while the lower left

inset shows the cell-to-PLB interactions with Collagen channel hidden. The cells are stretched out and form interactions with N-Cadherin PLB. We compare the hMSC-to-PLB interaction area from day 0 to day 1 in PLB/Collagen/hMSC matrices and find out the interaction area per cell goes up 10 fold in surface contact analysis of 20 randomly selected microspheres. PEGylated microshpheres (no lipid, no N-Cadherin), the control beads in the same 3D construct gave 5 fold less interaction area in Day 1 culture compare to hMSC-to-PLB interactions in day 1. In this case, the increase of cell to PLB interaction area shows the is consistent with the effect of the adhesion protein N-Cadherin displayed on the PLB surface.

Figure 4-8 gives another 3D CLSM reconstruction of hMSCs in N-cadherin proteolipobead/Collagen-I 3D construct in 63X meganification. This assembly is with proteolipobead-displayed N-Cadherin localized with Anti-N-Cadherin-phycoerytherin (red) and the hMSCs stained with Calcein-AM (green). Panel A is a 3D image of a representative region at Day 1 within a collagen-1 3D scaffold with three proteolipobeads with substantial cell to surface interactions. Panels B through D show individual z-sections with projections onto the X-Z and Y-Z planes at right and bottom from XY and X-Z orthogonal slices from the planes indicated by the dotted crosshair intersection in the 3D reconstruction. The anti-N-Cadherin-Phycoerytherin was formed uniform and smooth lipid bilayer at the surface of PLBs, shown as the equatorial confocal scanning images. The contact area in X-Z, Y-Z and X-Z projections (side and bottom panel) give different perspectives of the cell to PLB's interactions. In figure 4-9 a zoomed in view of a representative MSC-N-Cadherin PLB interaction is shown for three cells and a single N-Cad-PLB.

Figure 4-10 A shows a histogram and statistical analysis of 17 randomly selected N-Cad-PLBs (and n=42 interacting MSCs) at day 1 gave an average area per contact value of

296.2 ± 21.3 μm^2/cell (Avg ± Standard Error = SD/√n). The number of cells contacting each PLB was 2.5 ± 0.8, with the N-cadherin (anti-N-cadherin-PE detected) average percent coverage from to be 80.6±10.8%, slightly less than the percent microsphere lipid coverage (84.1±14.8%,). The PLBs were largely intact, although some evidence for lipid bilayer loss or damage was evidenced. Shown in panel 4-10B is a histogram of the contacting MSC cell nucleus to N-Cadherin PLB distance versus frequency of occurrence, which gave an average value of 18.3±1.7 μm. Panel C shows the correlation of MSC-PLB distance versus MSC-PLB interaction area. Greater than 81% (9 of 11) of the large contacts over 400 μm^2 were from MSC-nuclei-PLB distances less than 15 μm.

In a fraction of the MSCs interacting with the PLBs (4 out of 42 MSCs), images consistent with PLB-to-MSC biomembrane fusion were evidenced. Figure 4-11 displays 3D reconstructions of a PLB-MSC in which biomembrane fusion appeared to have occurred. Panel A is a merging of DiD Lipid tracer fluorescence (blue) with N-Cadherin detected by anti-N-Cad-PE (red), with Panel B showing only of N-Cadherin detected by anti-N-Cad-PE (red), Panel C is the overlay of the green (MSCs), red and blue channels with corresponding XZ and YZ orthogonal views from the dotted sectioning line. The DiD fluorescence extends from the PLB to the cell in two of the five cells interacting with the two N-Cad PLBs shown. More importantly, the distribution of N-Cadherin detected (shown in Panel B) is consistent with transfer of N-Cadherin-Fc-His_6 from the tailored PLB assembly to the cell periphery of a live human mesenchymal stem cell. Other MSCs interacting strongly with the same PLB assembly do not show similar loading of DiD tracer and N-Cadherin-Fc-His_6 display at their cell periphery, essentially serving as negative controls to fusion and N-cadherin protein transfer. In multiple hybrid constructs, containing hundreds of cells, we did not find any MSCs containing DiD

that were not directly in contact with N-Cadherin PLBs. This apparent fusion process and transfer of DiD probe and N-Cadherin is consistent with lateral lipid mobility in the PLB structures. Further studies of this are warranted.

Figure 4-12 gives a 3D display of MSC-N-Cadherin PLB interactions with apparent PLB-MSC fusion highlighting delivery of N-Cadherin to the plasma membrane of live MSCs. Panels A, B and C are individual Z-sections in the same XY plane (DiD lipid tracer (blue:A); anti-Ncadherin-PE; (B:red) and Calcein-AM: C:green). Image line profiles are extracted as indicated by the horizontal arrows and displayed as traces in the central inset (DiD: top; Anti-Ncadherin-PE: middle; Calcien-AM: bottom), the X axis indicates voxel number. Panel D displays the same Z-section in 3D with the intensity axis indicating where high levels N-cadherin is stained with anti-Ncadherin-PE (red). The left arrow points at the fused MSC and the right side arrow points at a MSC interacting with the PLB that did not fuse.

Conclusions

The main conclusions for this chapter are the following:

1. We have successfully fabricated N-Cadherin PLBs containing lipid tracers. Characterizations of N-Cadherin PLBs were analyzed via confocal microscopy and flow cytometry. N-Cadherin ligand display was quantified using MESF calibration beads via FACS analysis.

2. We have constructed and characterized novel microsphere-collagen hybrid scaffolds and uniquely identified encoded biomembrane assemblies within the hybrid scaffolds.

3. We have seeded hMSCs in hybrid scaffolds and measured 3D structures. Significant increases in cell-PLB interactions have been examined and quantified using confocal scanning and 3D reconstruction.

4. Evidence of PLBs transfer of N-Cadherin and DiD probe to a minor fraction of live cells

further confirms the lateral fluidity of lipid bilayer.

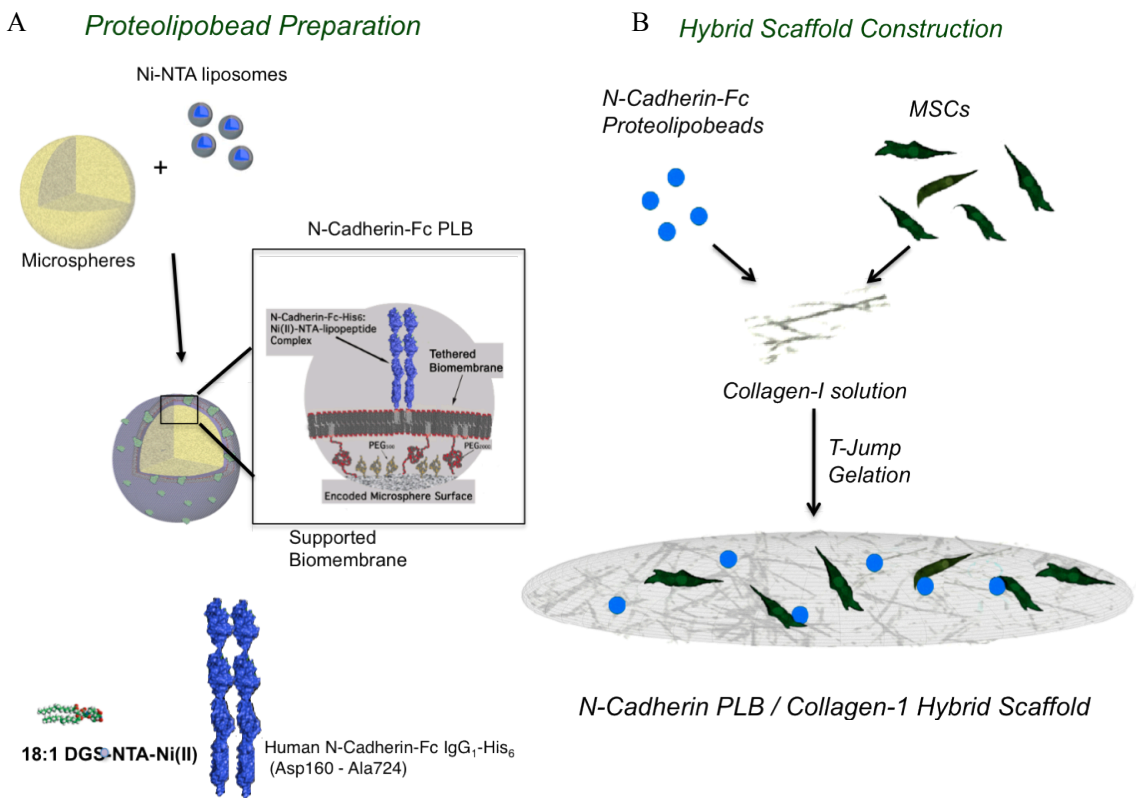

Figure 4-1. Schematic flow chart of Proteolipobead preparation (A) and construction of hybrid scaffold (B)

Barcode	Size (µm)	AF514-SA	A633-SA	Lipid Composition
A	4.7	+	-	10% Ni-NTA-PE 0.01% DiO
B	4.7	+	+	5% Ni-NTA-PE 0.01% DiO
C	4.7	-	+	1% Ni-NTA-PE 0.01% DiO
A'	2.8	+	-	10% Ni-NTA-PE 0.01% DiO
B'	2.8	+	+	5% Ni-NTA-PE 0.01% DiO
C'	2.8	-	+	1% Ni-NTA-PE 0.01% DiO

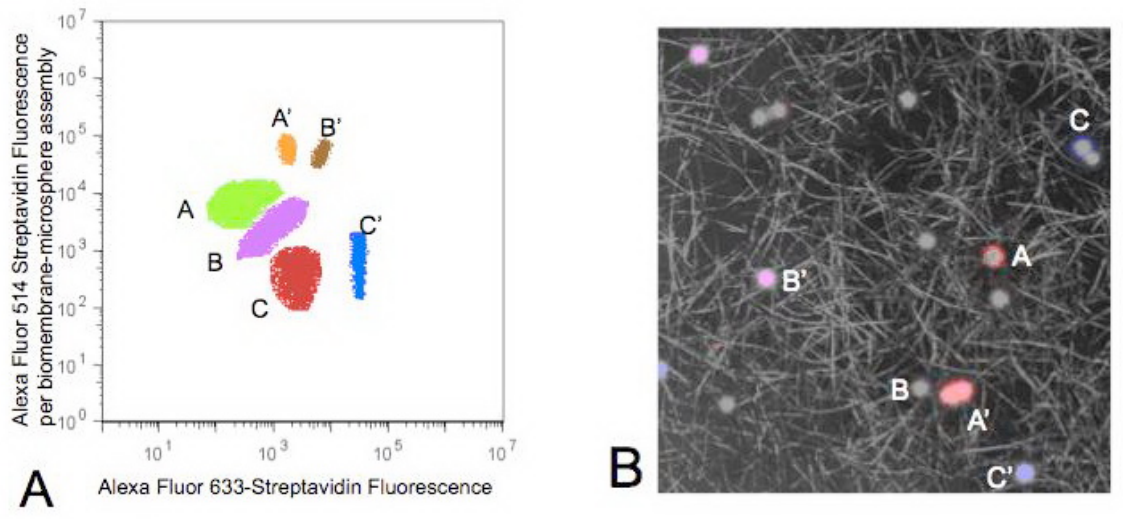

Figure 4-2. Prototypical encoded lipobead assemblies characterized and uniquely identified within 3D collagen-1 gels. Panel A is the flow cytometry characterization of the six barcodes based on streptavidin-alexafluor633 and streptavidin-alexaFluor514 labeling. Panel B is a 3D reconstruction of the barcoded beads identified by size and fluorescence within the collagen-I gel.

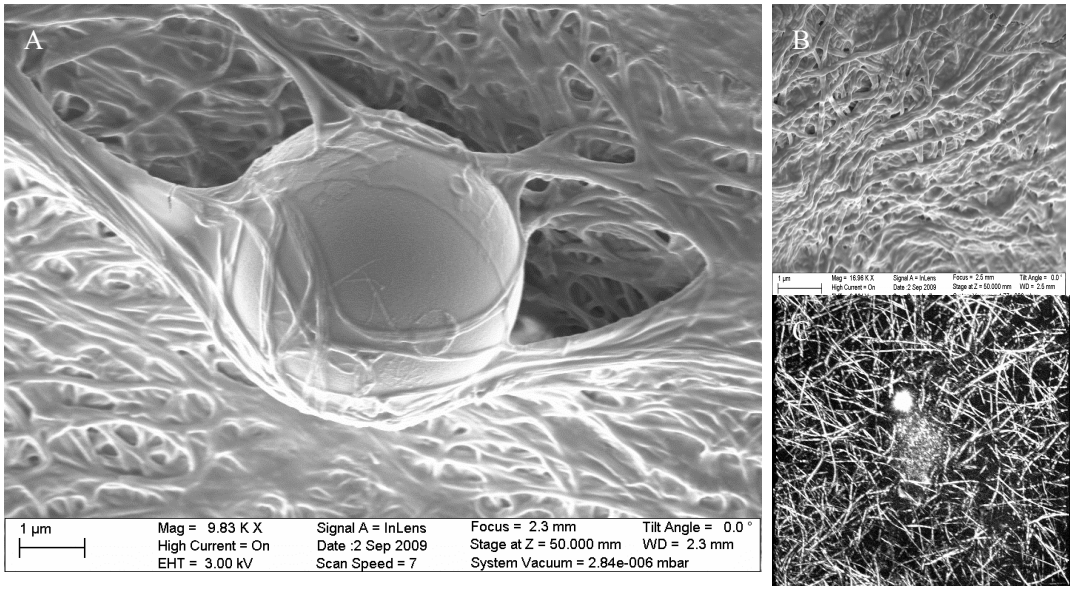

Figure 4-3. SEM image of microsphere-supported biomembran in collagen I hybrid (A), SEM image of gross fibrils of collagen I matrix (B), Confocal reflection image of a representative stem cell in collagen fibril. Scale bar: 1 µm

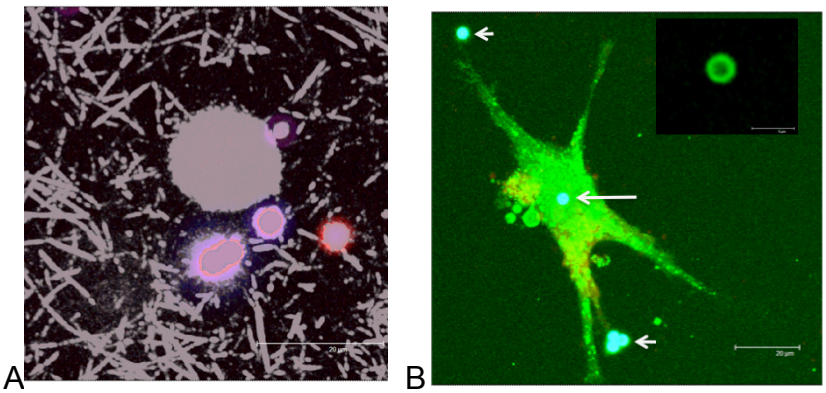

Figure 4-4. 3D reconstructions of representative hMSCs in microsphere-collagen-I hybrid scaffolds. Panel A was taken 2 hours after cell seeding; Panel B was acquired 2 days after seeding. The inset of panel B is the equatorial Z section image of the DiO tracer in the intact lipid bilayer of the microsphere at top left.

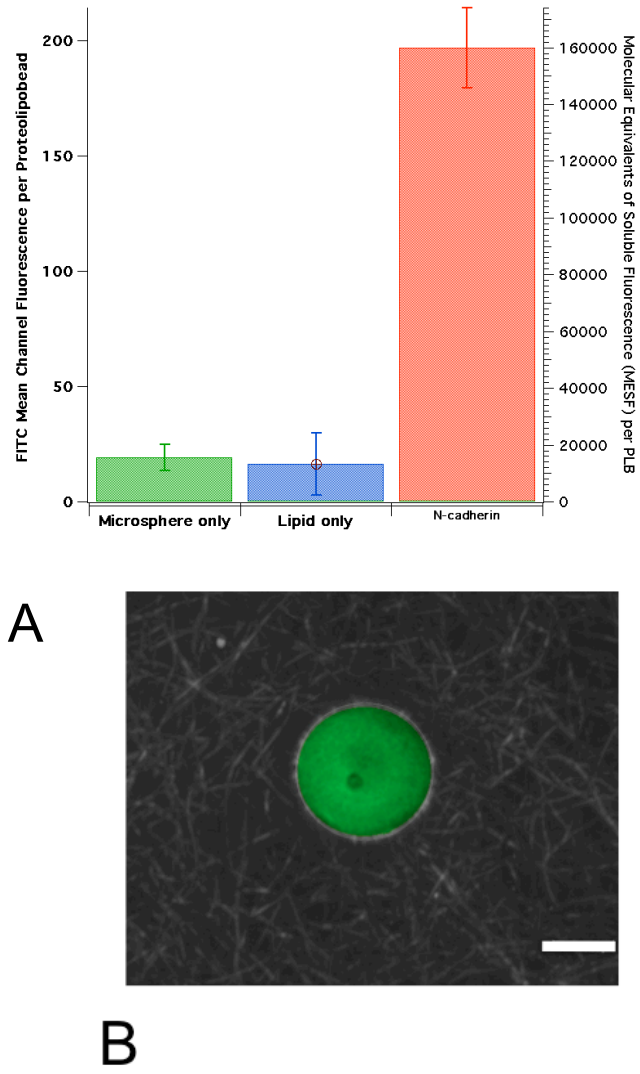

Figure 4-5. Characterization of Ligand Display on N-Cadherin Proteolipobeads. Top panel A consists of cytofluorograms from populations of microsphere assemblies treated with Anti-N-Cadherin-FITC to detect ligand display; the green bar (left) was from bare SiO2 microspheres (negative control); the blue bar (middle) was from Ni^{2+}NTA-DGS proteolipobeads not complexed with N-Cadherin-Fc-His_6 (negative control); the red bar (right) is from N-Cadherin-Fc-His_6-Ni^{2+}NTA-DGS proteolipobeads, yielding 20 fold greater detected level of N-Cadherin relative to the controls. The bottom panel B is a composite 3D reconstruction of displayed N-

Cadherin on a representative proteolipobead detected by Anti-N-Cad-FITC (green) within a collagen-I matrix (grey: reflection confocal imaging) scale bar 10 μm

Confocal 3D reconstruction Day 0 **Confocal 3D reconstruction Day 1**

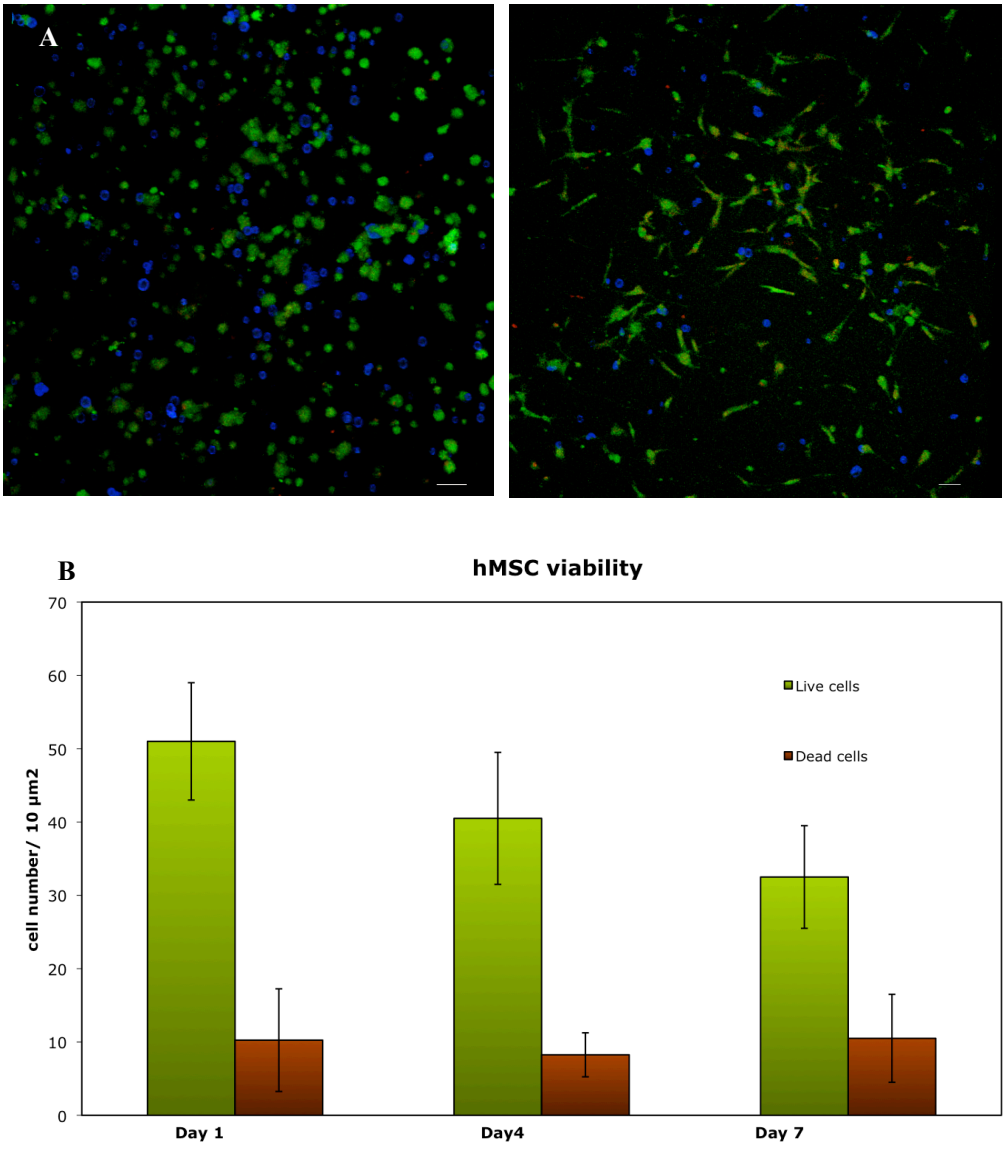

Figure 4-6. A. Representative Confocal 3D reconstruction of Collagen-MSC-PLB hybrid system at day 0 and day 1; and B, Cell viability in percentage at day 1, Day 4 and Day 7

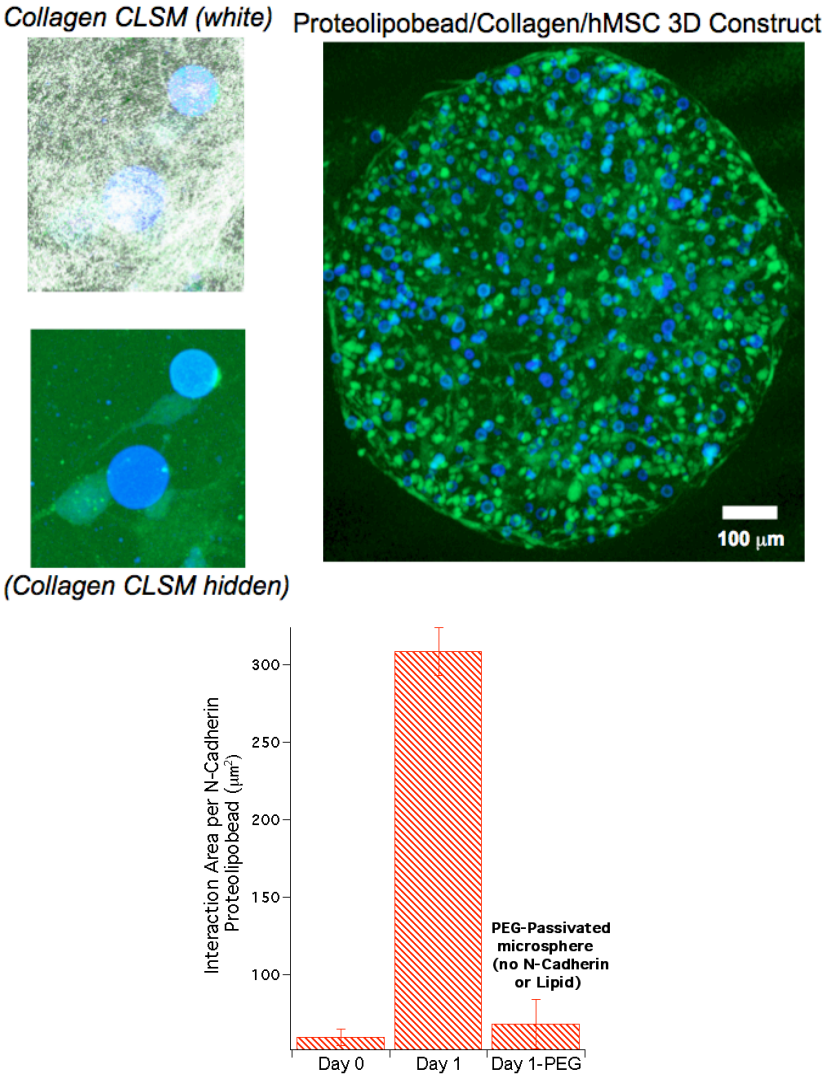

Figure 4-7. 3D CLSM reconstruction of hMSCs in N-cadherin proteolipobead/Collagen-I 3D constructs (N-cadherin proteolipobeads (blue) hMSCs (green), collagen fibers (white)). The inset is at 63X magnification. The bar chart shows the interaction area between hMSCs and microsphere assemblies within the 3D matrix. The hMSC interaction area goes up > 5-fold from day 0 to day 1 for N-Cadherin proteolipobeads when the cell processes form; (negative) control microspheres included in the same 3D construct that were passivated with PEGylated surfaces (no lipid, no N-Cadherin) gave ~4-fold less interaction area.

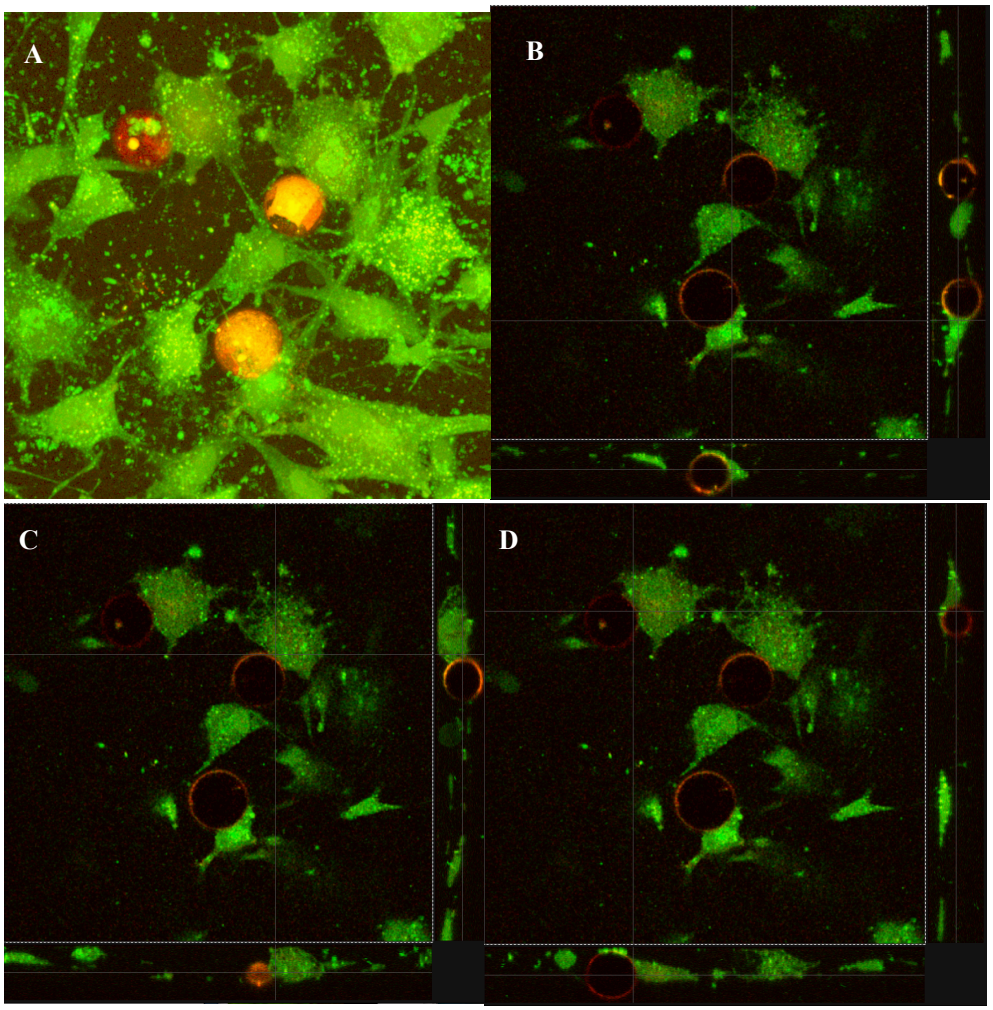

Figure 4-8. 3D CLSM reconstruction of hMSCs in N-cadherin proteolipobead/Collagen-I 3D constructs with the proteolipobead-displayed N-Cadherin localized with Anti-N-Cadherin-phycoerytherin (red) and the hMSCs stained with Calcein-AM (green). Panel A is a 3D image of a representative region at Day 1 within a collagen-1 3D scaffold with three proteolipobeads with substantial cell to surface interactions. Panels B through D show individual z-sections with projections onto the X-Z and Y-Z planes at right and bottom from XY and X-Z orthogonal slices from the planes indicated by the dotted crosshair intersection in the 3D reconstruction.

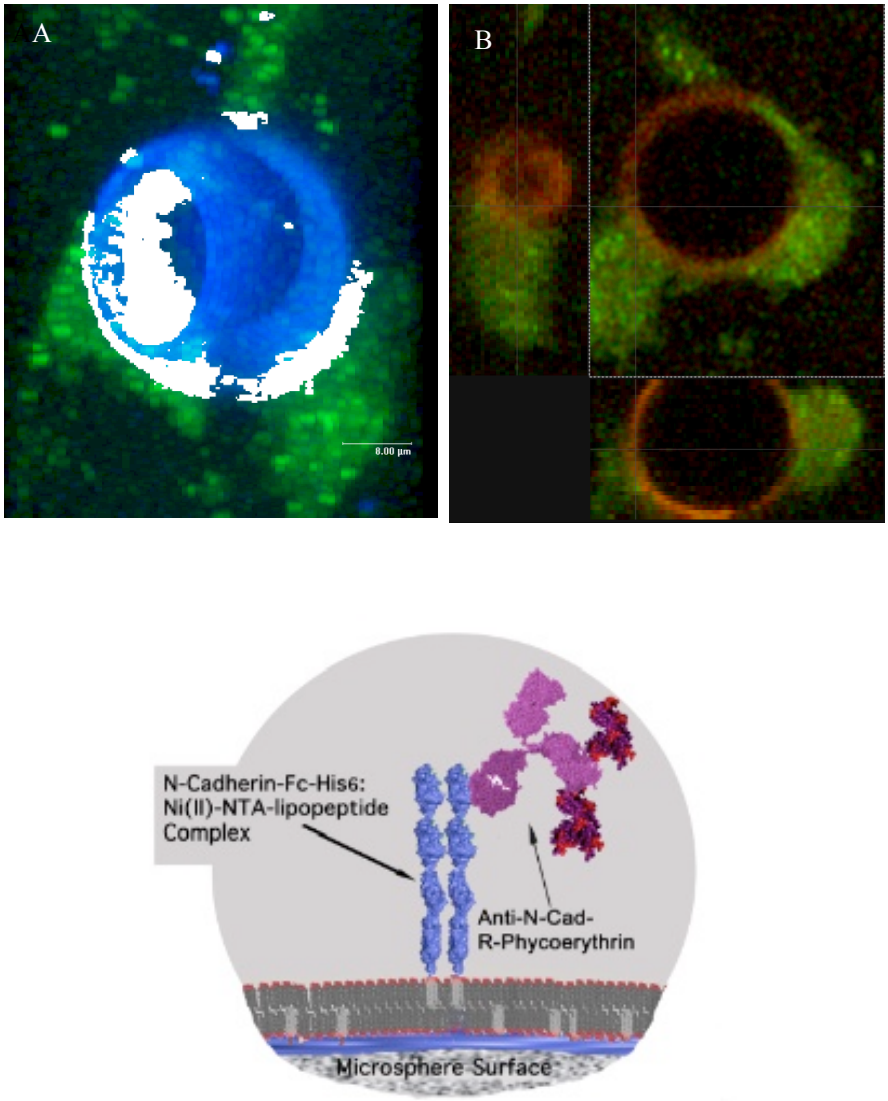

Figure 4-9. 3D display of MSC-N-Cadherin PLB interactions. 3D CLSM reconstruction of hMSCs in N-cadherin proteolipobead/Collagen-I 3D constructs with the proteolipobead-displayed hMSCs stained with Calcein-AM (green). Panel A show the interactions of three MSCs at the PLB interface (Lipid stain is blue: DiD lipid tracer), the white regions are the MSC-N-Cadherin PLB interactions in 3D. Panel B displays the N-cadherin stained with anti-Ncadherin-PE (red), with XZ and YZ projection views.

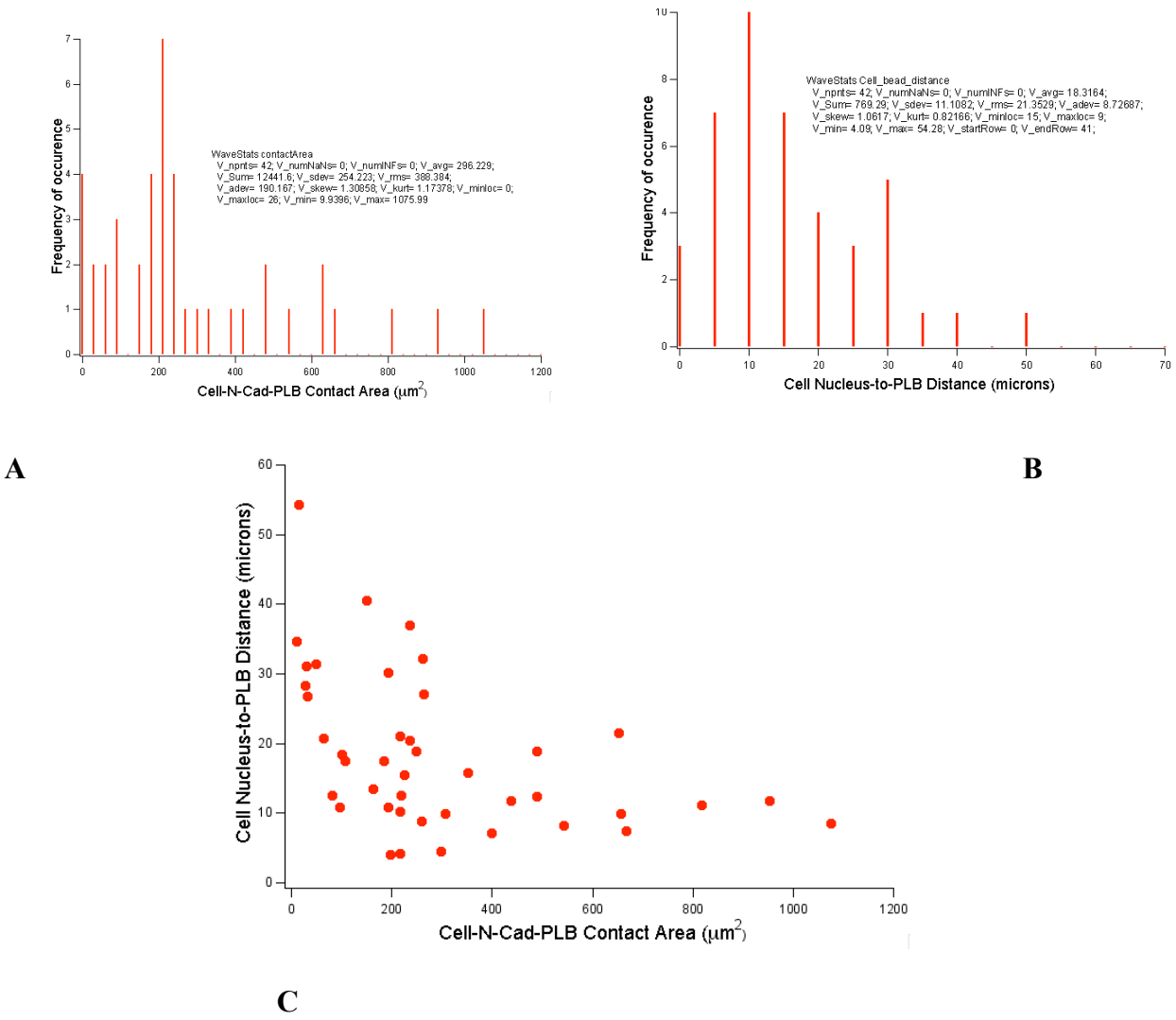

Figure 4-10. Statistical analysis of MSC-N-Cadherin PLB interactions. Histograms of MSC-N-Cadherin PLB contact area (A) and the MSC nucleus-to-N-Cadherin PLB distance. Panel (B) a plot of MSC-N-Cadherin PLB interaction contact area versus MSC nucleus-to-N-Cadherin PLB distance is given in (C).

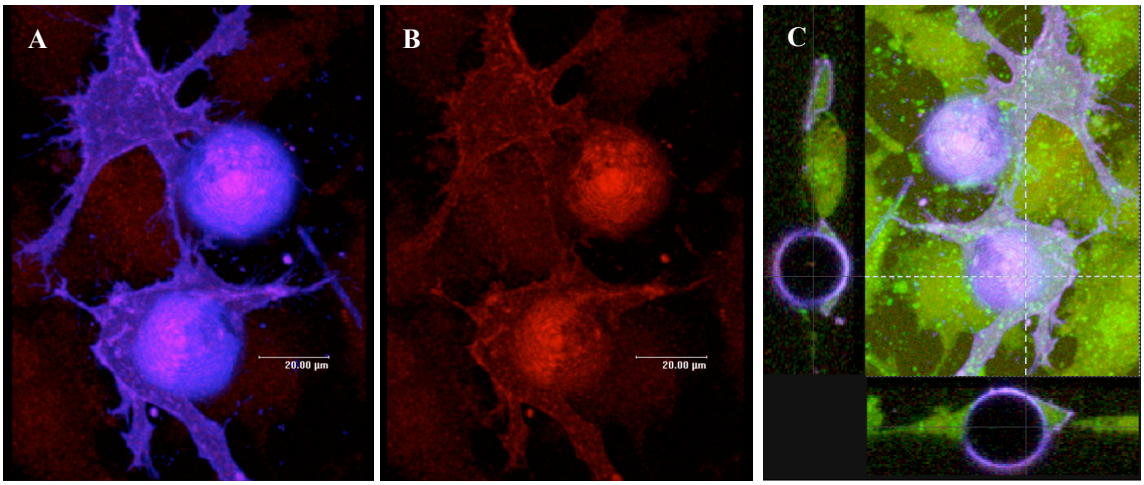

Figure 4-11. 3D display of MSC-N-Cadherin PLB interactions with apparent PLB-MSC fusion. 3D CLSM reconstruction of hMSCs within N-cadherin proteolipobead/Collagen-I 3D constructs with the proteolipobead-displayed hMSCs. Panel A show the interactions of MSCs at the PLB interface (Lipid stain is blue: DiD lipid tracer; anti-Ncadherin-PE; red), Panel B displays the N-cadherin stained with anti-Ncadherin-PE (red), Panel C displays the 3D reconstruction with the green (MSCs), red (anti-N-Cad-PE) and blue channels (DiD) with projections onto the X-Z and Y-Z planes at right and bottom from XY and X-Z orthogonal slices at the planes indicated by the dotted crosshair intersection in the 3D reconstruction.

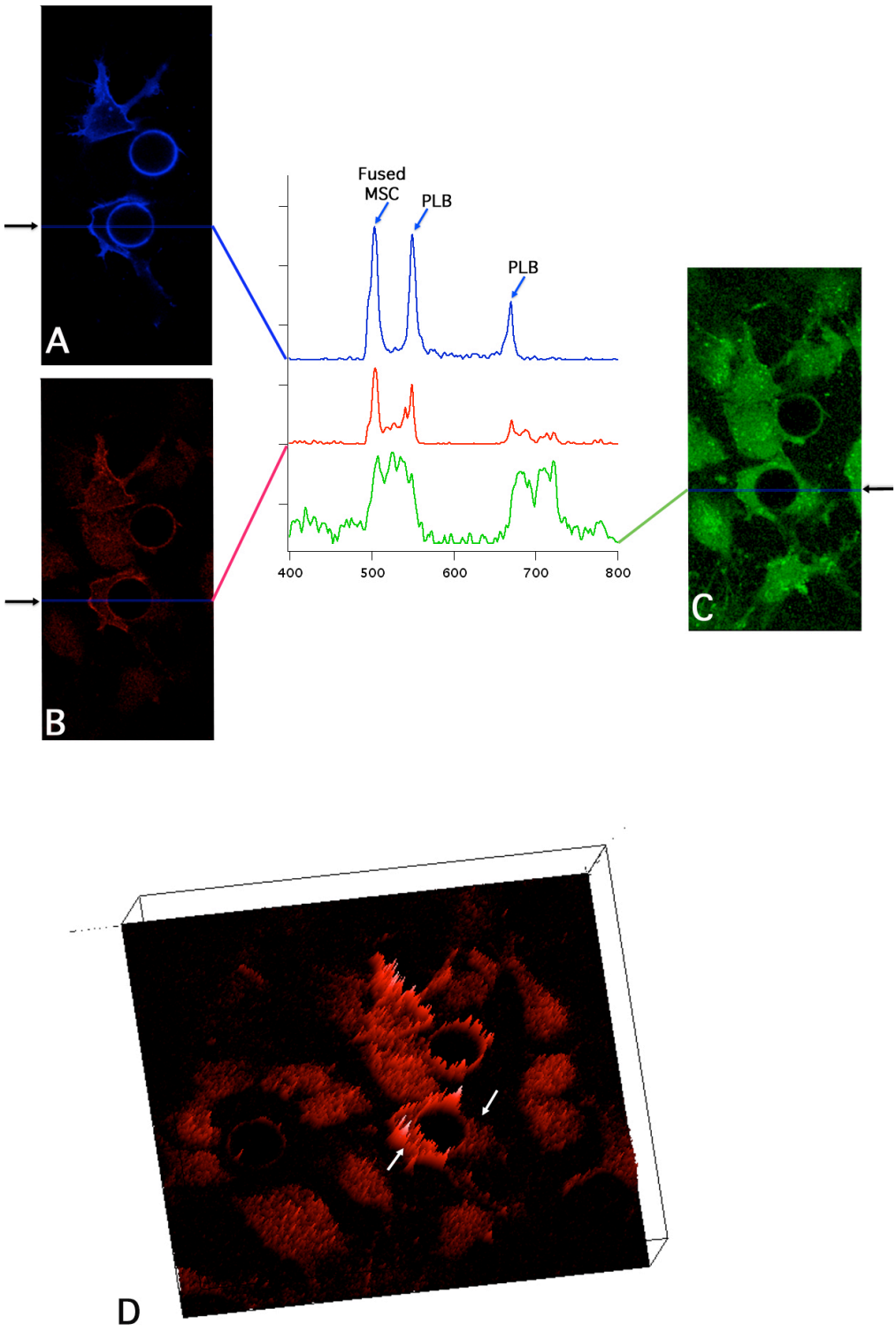

Figure 4-12. 3D display of MSC-N-Cadherin PLB interactions with apparent PLB-MSC fusion

highlighting delivery of N-Cadherin to the plasma membrane of live MSCs. Panels A, B and C are individual Z-sections in the same XY plane (DiD lipid tracer (blue:A); anti-Ncadherin-PE; (B:red) and Calcein-AM: C:green). Image line profiles are extracted as indicated by the horizontal arrows and displayed as traces in the central inset (DiD: top; Anti-Ncadherin-PE: middle; Calcien-AM: bottom), the X axis indicates voxel number. Panel D displays the same Z-section in 3D with the intensity axis indicating where high levels N-cadherin is stained with anti-Ncadherin-PE (red). The left arrow points at the fused MSC and the right side arrow points at a MSC interacting with the PLB that did not fuse.

Chapter 5

Conclusion and future work

Biological systems are becoming an important source of both inspiration and motivation for the design and construction of novel materials. Cell adhesion molecules exhibit unique functional capabilities with materials having desired physical properties. The current thesis serves as a primer for a new method that can be used to display ligands in supported lipid bilayers via proteolipobead complexes.

Overall objectives of this project are as follows: (1) formation of untethered and tether supported lipid bilayers on spherical particles, (2) characterization and comparison the tether supported structures with regular untethered beads via confocal FRAP, (3) construction of PDR5-GFP proteolipobeads and N-Cadherin proteolipobeads, (4) characterization of N-Cadherin density on proteolipobeads via FACS, (5) unique identification of proteolipobeads in collagen scaffolds by sizes and colors, (6) to seed hMSCs into hybrid scaffolds and measure 3D structures and cell-to-proteolipobead interactions.

Our major conclusions of this thesis project are summarized below:

Microsphere-supported biomembrane were formed on microspheres, size range from 5 to 30 microns. Assemblies were characterized by confocal imaging, FRAP, and FACS.

Transporter protein PDR5-GFP were isolated from yeast cell culture and purified under different scales. We developed the novel method of synthesizing the proteolipobeads assemblies with active functional N-Cadherin proteins and characterized the N-Cadherin density on the proteolipobeads surfaces via FACS and confocal microscopy. Preliminary evidence for microsphere-AAO filter fused systems was obtained.

We have constructed and characterized novel proteolipobead-collagen hybrid scaffolds and created uniquely identified encoded biomembrane assemblies within the hybrid scaffolds.

We have also examined 3D structures of collagen-MSC-PLB hybrid scaffolds. The

interactions between cells and PLBs were measured and cell growth and viability were characterized in 3D by confocal microscopy.

The motivation behind this work is to go beyond "flat biology" and the biomimicry stem cell environment in 3D niche to increase the complexity and diversity of *in vitro* models. These systems are to be used to uncover and understand the important molecular interactions involved in stem cell differentiation, quiescence and proliferation. This information can be integrated into improvements in 3D tissue scaffold design that could lead to new and effective biomaterials for regenerative medicine. So far we have successfully fabricated lipid bilayer assemblies on modified silica microspheres and loaded N-Cadherin proteolipobeads into hMSC 3D scaffolds. We have reached the proof-of-concept stage of displaying N-Cadherin ligands within 3D stem cell scaffolds. The future work of this project in light of the findings detailed in this dissertation entails the following:

(1) Formation of PEG tethered PLBs on N-Cadherin functional surfaces and characterize the tethered PLBs fluidity by FRAP.

(2) Study the effect of proteolipobead-displayed ligands of hMSC differentiation, migration and proliferation using different concentration of proteolipobeads and other matrix formulations such as natural and synthetic hydrogels.

(3) Further investigations of PLB-to-MSC fusions.

(4) Introduction of other ligands such as TGFβ receptor into the PLB-matrix hybrid scaffolds.

References

1. Helmut Jungwirth, K.K., *Yeast ABC transporters - A tale of sex, stress, drugs and aging.* FESB letters, 2006. **2006**(580): p. 1131-1138.
2. WALMSLEY, M.I.B.-W.a.A.R., *The structure and function of drug pumps.* TRENDS in MicroBiology, 2001. **9**(2): p. 71-78.
3. M. Ines BORGES-WALMSLEY, K.S.M.a.A.R.W., *structure and function of efflux pumps that confer resistance to drugs.* Biochemistry Journal, 2003. **2003**(376): p. 313-338.
4. Yamaguchi, S.M.a.A., *Multidrug-exporting secondary transporters.* Current Opinion in Structural Biology, 2003. **2003**(13): p. 443-452.
5. Srivastava, L.K., et al., *Reconstitution of affinity-purified dopamine D2 receptor binding activities by specific lipids.* Biochim Biophys Acta, 1987. **900**(2): p. 175-82.
6. Chattopadhyay, A., et al., *Role of cholesterol in ligand binding and G-protein coupling of serotonin1A receptors solubilized from bovine hippocampus.* Biochem Biophys Res Commun, 2005. **327**(4): p. 1036-41.
7. Rajendra Prasad, S.P., *Physiological functions of multidrug transporters in yeast.* Current Science, 2004. **86**(1): p. 62-73.
8. Tamm, L.K. and H.M. McConnell, *Supported phospholipid bilayers.* Biophys J, 1985. **47**(1): p. 105-13.
9. Gregoriadis, G. and A.T. Florence, *Liposomes in drug delivery. Clinical, diagnostic and ophthalmic potential.* Drugs, 1993. **45**(1): p. 15-28.
10. Ollivon, M., et al., *Vesicle reconstitution from lipid-detergent mixed micelles.* Biochim Biophys Acta, 2000. **1508**(1-2): p. 34-50.
11. Deleers, M. and W.J. Malaisse, *Binding of hypoglycaemic sulphonylureas to an artificial phospholipid bilayer.* Diabetologia, 1984. **26**(1): p. 55-9.
12. Malaisse, W.J. and B. Dard-Brunelle, *Binding of tritiated S21403 to an artificial phospholipid bilayer.* Res Commun Mol Pathol Pharmacol, 1999. **103**(3): p. 269-74.
13. Olson, F., et al., *Preparation of liposomes of defined size distribution by extrusion through polycarbonate membranes.* Biochim Biophys Acta, 1979. **557**(1): p. 9-23.
14. Bangham, A.D., *Liposomes: realizing their promise.* Hosp Pract (Off Ed), 1992. **27**(12): p. 51-6, 61-2.
15. Winterhalter, M. and D.D. Lasic, *Liposome stability and formation: experimental parameters and theories on the size distribution.* Chem Phys Lipids, 1993. **64**(1-3): p. 35-43.
16. Woodle, M.C., et al., *Sterically stabilized liposomes. Reduction in electrophoretic mobility but not electrostatic surface potential.* Biophys J, 1992. **61**(4): p. 902-10.
17. Lesieur, S., et al., *Size analysis and stability study of lipid vesicles by high-performance gel exclusion chromatography, turbidity, and dynamic light scattering.* Anal Biochem, 1991. **192**(2): p. 334-43.
18. Paternostre, M., et al., *Solubilization and reconstitution of vesicular stomatitis virus envelope using octylglucoside.* Biophys J, 1997. **72**(4): p. 1683-94.
19. Decottignies, A., P. Zarzov, and P. Nurse, *In vivo localisation of fission yeast cyclin-dependent kinase cdc2p and cyclin B cdc13p during mitosis and meiosis.* J Cell Sci, 2001. **114**(Pt 14): p. 2627-40.
20. Braeckmans, K., et al., *Three- dimensional fluorescence recovery after*

photobleaching with the confocal scanning laser microscope. Biophys J, 2003. **85**(4): p. 2240-52.
21. Tamm, L.K., *Lateral diffusion and fluorescence microscope studies on a monoclonal antibody specifically bound to supported phospholipid bilayers.* Biochemistry, 1988. **27**(5): p. 1450-7.
22. Axelrod, D., et al., *Mobility measurement by analysis of fluorescence photobleaching recovery kinetics.* Biophys J, 1976. **16**(9): p. 1055-69.
23. Schlessinger, J., et al., *Lateral transport on cell membranes: mobility of concanavalin A receptors on myoblasts.* Proc Natl Acad Sci U S A, 1976. **73**(7): p. 2409-13.
24. Tsuji, A. and S. Ohnishi, *Restriction of the lateral motion of band 3 in the erythrocyte membrane by the cytoskeletal network: dependence on spectrin association state.* Biochemistry, 1986. **25**(20): p. 6133-9.
25. Nolan, J.P., et al., *Flow cytometry: a versatile tool for all phases of drug discovery.* Drug Discov Today, 1999. **4**(4): p. 173-180.
26. Teotia, S. and M.N. Gupta, *Purification of alpha-amylases using magnetic alginate beads.* Appl Biochem Biotechnol, 2001. **90**(3): p. 211-20.
27. Safarik, I. and M. Safarikova, *Use of magnetic techniques for the isolation of cells.* J Chromatogr B Biomed Sci Appl, 1999. **722**(1-2): p. 33-53.
28. Ghaemmaghami, S., et al., *Global analysis of protein expression in yeast.* Nature, 2003. **425**(6959): p. 737-41.
29. Chen, Y. and S.M. Simon, *In situ biochemical demonstration that P-glycoprotein is a drug efflux pump with broad specificity.* J Cell Biol, 2000. **148**(5): p. 863-70.
30. Ivo Safarik, M.S., *Use of magnetic tehniques for the isolation of cells.* Journal of Chromatography, 1999. **722**(1999): p. 33-53.
31. Takuya Kinoshita, S.S., Yoshiteru Mizukoshi, yohei Otome, Takashi Nakagawa, Kenji Okitsu, Takao A. Yamamoto, *Magnetic separation of amino acids by gold/iron-oxide composite nanoparticles synthesized by gamma-ray irradiation.* Journal of Magnetism and Magnetic Materials, 2005. **293**: p. 106-110.
32. Ivo Safarik, M.S., *Magnetic Techniques for the isolation and purification of proteins and Peptides.* BioMagnetic Research and Technology, 2004. **2**: p. 2-17.
33. M. Schuster, E.W., C. Ortner, K. Graumann, A. Jungbauer, F. Hammerschmid and G. Werner, *Short cut of protein purification by integration of cell-disrupture and affinity extraction.* Bioseparation, 2000. **9**(2000): p. 59-67.
34. Evan, G.I., et al., *Isolation of monoclonal antibodies specific for human c-myc proto-oncogene product.* Mol Cell Biol, 1985. **5**(12): p. 3610-6.
35. Field, J., et al., *Purification of a RAS-responsive adenylyl cyclase complex from Saccharomyces cerevisiae by use of an epitope addition method.* Mol Cell Biol, 1988. **8**(5): p. 2159-65.
36. Dickinson, J.d.D.A.a.H., *Affinity Chromatographic Purification of Antibodies to a Biotinylated Fusion Protein Expressed in Escherichcia Coli.* Protein Expression and Purification, 1997. **12**(1998): p. 138-143.
37. Ian J. Bruce, J.T., Michael Todd, Martin J. Davies, Enrico Borioni, Claudio Sangregorio and Tapas Sen., *Synthesis, characterisation and application of silica-magnetite nanocomposites.* Journal of Magnetism and Magnetic Materials, 2004. **284**: p. 145-160.
38. Gilljam, G., K. Siridewa, and L. Hammar, *Purification of simian immunodeficiency virus, SIVMAC251, and of its external envelope glycoprotein, gp148.* J Chromatogr

A, 1994. **675**(1-2): p. 89-100.
39. Woo-Jae Chung, M.-S.K., Suhyung Cho, Sung-Soo Park, Jong-Ho Kim, Byung-Gee Kim, Yoon-Sik Lee, *Microaffinity purification of protein based on photolytic elution: Toward an efficient microbead affinity chromatography on a chip.* Elctropphoresis, 2005. **2005**(26): p. 694-702.
40. Mamnun, Y.M., C. Schuller, and K. Kuchler, *Expression regulation of the yeast PDR5 ATP-binding cassette (ABC) transporter suggests a role in cellular detoxification during the exponential growth phase.* FEBS Lett, 2004. **559**(1-3): p. 111-7.
41. Thid, D., et al., *Supported phospholipid bilayers as a platform for neural progenitor cell culture.* J Biomed Mater Res A, 2008. **84**(4): p. 940-53.
42. Sackmann, E., *Supported membranes: scientific and practical applications.* Science, 1996. **271**(5245): p. 43-8.
43. Hirn, R., et al., *The effect of S-layer protein adsorption and crystallization on the collective motion of a planar lipid bilayer studied by dynamic light scattering.* Biophys J, 1999. **77**(4): p. 2066-74.
44. Wagner, M.L. and L.K. Tamm, *Tethered polymer-supported planar lipid bilayers for reconstitution of integral membrane proteins: silane-polyethyleneglycol-lipid as a cushion and covalent linker.* Biophys J, 2000. **79**(3): p. 1400-14.
45. Kiessling, V. and L.K. Tamm, *Measuring distances in supported bilayers by fluorescence interference-contrast microscopy: polymer supports and SNARE proteins.* Biophys J, 2003. **84**(1): p. 408-18.
46. Thid, D., et al., *Issues of ligand accessibility and mobility in initial cell attachment.* Langmuir, 2007. **23**(23): p. 11693-704.
47. Benkoski, J.J. and F. Hook, *Lateral mobility of tethered vesicle-DNA assemblies.* J Phys Chem B, 2005. **109**(19): p. 9773-9.
48. Earley, M.C., et al., *Report from a workshop on multianalyte microsphere assays.* Cytometry, 2002. **50**(5): p. 239-42.
49. Lutolf, M.P. and H.M. Blau, *Artificial stem cell niches.* Adv Mater, 2009. **21**(32-33): p. 3255-68.
50. Dellatore, S.M., A.S. Garcia, and W.M. Miller, *Mimicking stem cell niches to increase stem cell expansion.* Curr Opin Biotechnol, 2008. **19**(5): p. 534-40.
51. Zhang, J., A. Skardal, and G.D. Prestwich, *Engineered extracellular matrices with cleavable crosslinkers for cell expansion and easy cell recovery.* Biomaterials, 2008. **29**(34): p. 4521-31.
52. Lutolf, M.P., et al., *Perturbation of single hematopoietic stem cell fates in artificial niches.* Integr Biol (Camb), 2009. **1**(1): p. 59-69.
53. Doran, M.R., et al., *Surface-bound stem cell factor and the promotion of hematopoietic cell expansion.* Biomaterials, 2009. **30**(25): p. 4047-52.
54. Kertesz, Z., et al., *In vitro expansion of long-term repopulating hematopoietic stem cells in the presence of immobilized Jagged-1 and early acting cytokines.* Cell Biol Int, 2006. **30**(5): p. 401-5.
55. Pittenger, M.F., et al., *Multilineage potential of adult human mesenchymal stem cells.* Science, 1999. **284**(5411): p. 143-7.
56. Li, J., et al., *Differential damage and recovery of human mesenchymal stem cells after exposure to chemotherapeutic agents.* Br J Haematol, 2004. **127**(3): p. 326-34.
57. Horwitz, E.M., et al., *Clarification of the nomenclature for MSC: The International*

Society for Cellular Therapy position statement. Cytotherapy, 2005. **7**(5): p. 393-5.
58. Hatta, K. and M. Takeichi, *Expression of N-cadherin adhesion molecules associated with early morphogenetic events in chick development.* Nature, 1986. **320**(6061): p. 447-9.
59. Perez, T.D., et al., *E-cadherin tethered to micropatterned supported lipid bilayers as a model for cell adhesion.* Langmuir, 2005. **21**(25): p. 11963-8.
60. Lambert, M., F. Padilla, and R.M. Mege, *Immobilized dimers of N-cadherin-Fc chimera mimic cadherin-mediated cell contact formation: contribution of both outside-in and inside-out signals.* J Cell Sci, 2000. **113** (12): p. 2207-19.
61. Tavella, S., et al., *N-CAM and N-cadherin expression during in vitro chondrogenesis.* Exp Cell Res, 1994. **215**(2): p. 354-62.
62. Oberlender, S.A. and R.S. Tuan, *Application of functional blocking antibodies. N-cadherin and chick embryonic limb development.* Methods Mol Biol, 2000. **137**: p. 37-42.
63. Oberlender, S.A. and R.S. Tuan, *Spatiotemporal profile of N-cadherin expression in the developing limb mesenchyme.* Cell Adhes Commun, 1994. **2**(6): p. 521-37.
64. Treiser, M.D., et al., *Profiling cell-biomaterial interactions via cell-based fluororeporter imaging.* Biotechniques, 2007. **43**(3): p. 361-6, 368.
65. Lutolf, M.P., *Integration column: artificial ECM: expanding the cell biology toolbox in 3D.* Integr Biol (Camb), 2009. **1**(3): p. 235-41.
66. Puech, P.H., H. Feracci, and F. Brochard-Wyart, *Adhesion between giant vesicles and supported bilayers decorated with chelated E-cadherin fragments.* Langmuir, 2004. **20**(22): p. 9763-8.
67. Nagaoka, M., et al., *Embryonic undifferentiated cells show scattering activity on a surface coated with immobilized E-cadherin.* J Cell Biochem, 2008. **103**(1): p. 296-310.
68. Wong, H.L., et al., *A 3D collagen microsphere culture system for GDNF-secreting HEK293 cells with enhanced protein productivity.* Biomaterials, 2007. **28**(35): p. 5369-80.
69. Semler, E.J., A. Dasgupta, and P.V. Moghe, *Cytomimetic engineering of hepatocyte morphogenesis and function by substrate-based presentation of acellular E-cadherin.* Tissue Eng, 2005. **11**(5-6): p. 734-50.
70. Flynn, L., et al., *Adipose tissue engineering in vivo with adipose-derived stem cells on naturally derived scaffolds.* J Biomed Mater Res A, 2009. **89**(4): p. 929-41.
71. Flynn, L. and K.A. Woodhouse, *Adipose tissue engineering with cells in engineered matrices.* Organogenesis, 2008. **4**(4): p. 228-35.
72. Liu, Y., et al., *Disulfide-crosslinked hyaluronan-gelatin sponge: growth of fibrous tissue in vivo.* J Biomed Mater Res A, 2004. **68**(1): p. 142-9.
73. Shu, X.Z., et al., *Disulfide-crosslinked hyaluronan-gelatin hydrogel films: a covalent mimic of the extracellular matrix for in vitro cell growth.* Biomaterials, 2003. **24**(21): p. 3825-34.
74. Shu, X.Z., et al., *Synthesis and evaluation of injectable, in situ crosslinkable synthetic extracellular matrices for tissue engineering.* J Biomed Mater Res A, 2006. **79**(4): p. 902-12.
75. Adams, C.L., W.J. Nelson, and S.J. Smith, *Quantitative analysis of cadherin-catenin-actin reorganization during development of cell-cell adhesion.* J Cell Biol, 1996. **135**(6 Pt 2): p. 1899-911.
76. Lauer, S.A. and J.P. Nolan, *Development and characterization of Ni-NTA-bearing microspheres.* Cytometry, 2002. **48**(3): p. 136-45.